

**3D MODELLING OF SUBSTRATE
INTEGRATED WAVEGUIDE (SIW) SENSOR
FOR CHARACTERIZATION OF DIELECTRIC
MATERIAL**

NURAZYYATI BINTI INAS

**BACHELOR OF ENGINEERING TECHNOLOGY
(ELECTRICAL) WITH HONORS**

UNIVERSITI MALAYSIA PAHANG

UNIVERSITI MALAYSIA PAHANG

DECLARATION OF THESIS AND COPYRIGHT

Author's Full Name : NURAZYYATI BINTI INAS
Date of Birth :
Title : 3D MODELLING OF SUBSTRATE INTEGRATED
WAVEGUIDE (SIW) SENSOR FOR
CHARACTERIZATION OF DIELECTRIC
MATERIAL
Academic Session : SEMESTER I ACADEMIC SESSION 2021/2022

I declare that this thesis is classified as:

- CONFIDENTIAL (Contains confidential information under the Official Secret Act 1997)*
 RESTRICTED (Contains restricted information as specified by the organization where research was done)*
 OPEN ACCESS I agree that my thesis to be published as online open access (Full Text)

I acknowledge that Universiti Malaysia Pahang reserves the following rights:


1. The Thesis is the Property of Universiti Malaysia Pahang
2. The Library of Universiti Malaysia Pahang has the right to make copies of the thesis for the purpose of research only.
3. The Library has the right to make copies of the thesis for academic exchange.

Certified by:

(Student's Signature)

New IC/Passport Number

Date: 21/2/2022



(Supervisor's Signature)

Name of Supervisor
TS. DR NURHAFIZAH BINTI
ABU TALIP@YUSOF

Date: 21/02/2022

NOTE : * If the thesis is CONFIDENTIAL or RESTRICTED, please attach a thesis declaration letter.



SUPERVISOR'S DECLARATION

I hereby declare that I have checked this thesis and, in my opinion, this thesis is adequate in terms of scope and quality for the award of the degree of Bachelor of Engineering Technology (Electrical) with Hons.

A handwritten signature in blue ink, appearing to be 'Nurhafizah', written over a horizontal line.

(Supervisor's Signature)

Full Name : Ts. Dr. Nurhafizah bt. Abu Talib Yusof
Position : Senior Lecturer
Date : 21/02/2022



STUDENT'S DECLARATION

I hereby declare that the work in this thesis is based on my original work except for quotations and citations which have been duly acknowledged. I also declare that it has not been previously or concurrently submitted for any other degree at Universiti Malaysia Pahang or any other institutions.

(Student's Signature)

Full Name : NURAZYYATI BINTI INAS

ID Number : TB18021

Date : 21/2/2022

3D MODELLING OF SUBSTRATE INTEGRATED
WAVEGUIDE (SIW) SENSOR FOR CHARACTERIZATION OF DIELECTRIC
MATERIAL

NURAZYYATI BINTI INAS

Thesis submitted in fulfillment of the requirements
for the award of the degree of
Bachelor Engineering Technology (Electrical) with Hons.

Faculty of Electrical & Electronics Engineering Technology
UNIVERSITI MALAYSIA PAHANG

FEBRUARY 2022

ACKNOWLEDGEMENTS

In the name of Allah, Most Gracious, Most Merciful.

Praise be to Allah SWT for the abundance of His grace, so that I can complete the thesis entitled 3D Modelling of Substrate Integrated Waveguide (SIW) for Characterization of Dielectric Material. This thesis is to fulfil one of the requirements for completing the study as well as to obtain a graduate degree in Bachelor's degree of Engineering Technology (Electrical), Faculty of Electric and Electronic Engineering Technology, Universiti Malaysia Pahang.

Sincere appreciation and gratitude to my beloved father, Inas bin Saidin and my dear mother, Norjiha binti Mohamed, who have poured all love and affection as well as moral attention. May Allah SWT grant mercy, grace, health, and blessings in this world and the hereafter for the kindness that has been given to me. Through this writing, allow me to express my gratitude and appreciation to:

1. Ts. Dr. Nurhafizah binti Abu Talip@Yusof is my supervisor who has spent a lot of time to providing instruction, input and guiding me in the preparation of this thesis. May Allah SWT repay all the kindness that has been given.
2. Muhammad Naim bin Aminuddin who is my groupmate for this project, thank you for the moral support, prayers and helping me to complete this thesis.
3. Nurul Hafizah binti Adnan and Intan Suraya Ahmad Ismail for always be there for me and for their enthusiasm and strong support.
4. Batch mates from Electrical Engineering Technology program who have provided helpful suggestions and encouragements.
5. Lastly, to various parties whose names have not been mentioned one by one, thank you for all the help given, their prayers provided me a constant source of inspiration.

Finally, I realize that in writing this thesis, is still far from being perfect. Therefore, I ask for suggestions and criticisms that are constructive for the sake of perfection and may be useful for all of us. Ameen.

ABSTRAK

Bahan dielektrik adalah sejenis bahan elektronik filem nipis yang digunakan dalam mikroelektronik. Peranti aktif, seperti transistor dan pengasingan elektrik mereka, seperti kapasitor, digunakan dalam pelbagai aplikasi. Bahan dielektrik permit tinggi digunakan untuk meningkatkan prestasi peranti semikonduktor. Pembangunan bahan telah bermula dengan penemuan resin termoplastik, poliamides dan lain-lain. Ini membawa kepada kemajuan teknik pencirian bahan seperti menggunakan pelbagai cara termasuk resonator planar dan substrat waveguide bersepadu (SIW). Pelbagai kaedah telah digunakan untuk pencirian bahan. Walau bagaimanapun, kaedah ini mempunyai isu-isu yang khusus untuk kegunaan mereka. Sebagai contoh, teknik yang memerlukan vakum tidak boleh digunakan untuk menganalisis cecair atau bahan kimia yang tidak menentu. Batasan ini bermaksud bahawa teknik tertentu mungkin mempunyai pelbagai aplikasi yang terhad. Dalam tesis ini, reka bentuk model baru Substrat Sensor Waveguide Bersepadu (SIW) untuk pencirian dielektrik dibentangkan. Untuk meningkatkan ketepatan sensor ini dalam mengekstrak ciri-ciri bahan dielektrik, parameter prestasi sensor ini dianalisis dan dinilai untuk memastikan prestasi menggunakan perisian CST. Mengenai pemodelan sensor, langkah-langkah bermula dengan pengesahan teknik pemodelan dari penyelidikan reka bentuk yang dilaporkan sebelumnya. Selepas teknik pemodelan disahkan, analisis untuk perubahan geometri dan dimensi seperti jarak pusat ke pusat 'a', diameter vias 'd' dan tempoh antara vias 'p', diperhatikan untuk memenuhi reka bentuk keperluan sensor ini. Keputusan analisis ini membawa kepada pemodelan reka bentuk sendiri, di mana resonan pada 5.02GHz yang meliputi julat G-band. Parameter penyebaran sensor ini adalah di bawah -10dB dalam G-band yang mewakili ciri-ciri prestasi yang baik sensor ini. Parameter simulasi dan penyebaran diukur mempunyai prestasi yang baik pada 5.02GHz dan 5.6GHz masing-masing yang kedua-dua frekuensi dilindungi dalam julat G-band. Juga, corak radiasi dianalisis untuk mengesahkan prestasi sensor. Kesimpulannya, sensor SIW direka pada G-band yang beroperasi pada frekuensi 5.02GHz dan corak radiasi yang baik dengan sidelobes -2.7dB.

ABSTRACT

Dielectrics materials are a type of thin-film electronic material that is used in microelectronics. Active devices, such as transistors and their electrical isolation, such as capacitors, are used in a wide range of applications. High permittivity dielectric materials are utilized to improve the performance of semiconductor devices. Material development has begun with the discovery of thermoplastic resins, polyamides etc. These lead to the advancement of material characterization techniques such as using a variety of ways including planar resonators and substrate integrated waveguide (SIW). Various methods have been used for material characterization. However, these methods have issues that are specific to their uses. For instance, techniques that require vacuum cannot be used for analysing liquid or volatile chemicals. This limitation means that a given technique may have a limited range of applications. In this thesis, a new model design Substrate Integrated Waveguide (SIW) sensor for characterization of dielectric is presented. In order to enhance the accuracy of this sensor in extracting dielectric characteristics of materials, the performance parameter of this sensor is analysed and evaluated to assure performance using CST software. Concerning the modelling of the sensor, the steps started with validation of modelling technique from previous reported design research. After the technique of modelling is verified, the analysis for geometrical and dimensional changes such as the centre-to-centre distance 'a', the diameter of vias 'd' and the period between the vias 'p', are observed to meet the requirement design of this sensor. These analysis results are led to the modelling of own design, where resonant at 5.02GHz which covered in G-band range. The scattering parameters of this sensor are below -10dB in G-band which representing the good performance characteristics of this sensor. The simulation and measured scattering parameter have a good performance at 5.02GHz and 5.6GHz respectively which both frequencies covered in G-band range. Also, radiation patterns are analysed in order to validate the performance of the sensor. For the conclusion, the SIW sensor is designed on G-band operating at the frequency of 5.02GHz and a good radiation pattern with sidelobes of -2.7dB.

TABLE OF CONTENT

DECLARATION	
TITLE PAGE	
ACKNOWLEDGEMENTS	ii
ABSTRAK	iii
ABSTRACT	iv
TABLE OF CONTENT	v
LIST OF TABLES	viii
LIST OF FIGURES	ix
LIST OF ABBREVIATIONS	xi
CHAPTER 1 INTRODUCTION	12
1.1 Project Background	12
1.2 Problem Statement	13
1.3 Objective	13
1.4 Scope of the project	14
1.5 Summary	14
CHAPTER 2 LITERATURE REVIEW	15
2.1 Introduction	15
2.2 Dielectric properties	15
2.3 Measuring Technique for Characterization of Dielectric Materials	17
2.4 Substrate Integrated Waveguide (SIW)	24
2.4.1 SIW Mechanism	25
2.4.2 Design Guidelines	27
2.5 Different Model of SIW from Previous Research	28

2.5.1	Model for Material Detection	28
2.6	Important Sensor Performance Parameter	31
2.6.1	Scattering Parameter	31
2.6.2	Directivity	34
CHAPTER 3 RESEARCH METHODOLOGY		35
3.1	Introduction	35
3.2	Flowchart	35
3.3	Numerical result	37
3.4	Consideration and design steps	37
3.5	Modelling of SIW Sensor	39
3.6	Analysis of Distance between 2 rows of vias of SIW sensor	44
3.7	Analysis of flaring angle of SIW sensor	45
3.8	Analysis of distance between 2 vias (pitch) of SIW sensor	46
3.9	Modelling of New SIW Sensor Design	47
3.10	Finalize design	48
3.11	Chapter Summary	49
CHAPTER 4 RESULTS AND DISCUSSIONS		50
4.1	Introduction	50
4.2	Result of Modelling of SIW Sensor	50
4.3	Result of Analysis of Distance Between 2 Rows of Vias of SIW Sensor	54
4.4	Result of Analysis of Flaring Angle of SIW Sensor	55
4.5	Result of Analysis of Distance Between 2 Via (Pitch) of SIW Sensor	55
4.6	Result of Modelling of New SIW Sensor Design	56
4.7	Result of Finalize Design	58

4.8	Chapter summary	60
	CHAPTER 5 CONCLUSION	61
5.1	Conclusion	61
	REFERENCES	62

LIST OF TABLES

Table 2.1	The resonant frequency of various standard dielectric samples	17
Table 2.2	Comparison of characterization technique	23
Table 2.3	Solid, powder and liquid detection with its antenna type used and working frequency	28
Table 3.1	Parameter of the SIW basic structure for Figure 3.2	40
Table 3.2	Parameter of the SIW basic structure for Figure 3.3	41
Table 3.3	Parameter of the SIW horn antenna structure for Figure 3.4	42
Table 3.4	Parameter of the SIW horn antenna structure for Figure 3.5	44
Table 3.5	Full dimension of design for 3 analysis above	47

LIST OF FIGURES

Figure 2.1	The frequency dependence of a hypothetical dielectric's permittivity.	18
Figure 2.2	A coaxial probe with flange.	19
Figure 2.3	Illustration of free space method for material characterization	20
Figure 2.4	Illustration of an encapsulation for the purpose of determining the properties of a free space liquid	20
Figure 2.5	Parallel Plate illustration method	21
Figure 2.6	Cavity resonator method illustration	22
Figure 2.7	Transmission line (waveguide) method illustration	22
Figure 2.8	(a) SIW perspective view structure; (b) SIW basic mode in cross-section view	24
Figure 2.9	Rectangular waveguide structure	25
Figure 2.10	Electromagnetic field distribution of TE mode.	26
Figure 2.11	Structure of conventional SIW Horn	30
Figure 2.12	RF relay model	32
Figure 2.13	S-parameter model	32
Figure 2.14	Far-field radiation patterns	34
Figure 3.1	Overall flowchart for modelling SIW and analyse the geometrical parameter of SIW sensor	36
Figure 3.2	(a) Design and (b) reproduce design of SIW basic structure from Tanvi [29]	40
Figure 3.3	(a) Design and (b) reproduce design of SIW basic structure from Shibu [30]	41
Figure 3.4	(a) Design and (b) reproduce design of SIW horn antenna structure from Tanvi [29]	42
Figure 3.5	(a) Design and (b) reproduce design of SIW horn antenna structure from Shibu [30]	43
Figure 3.6	Varied value of distance between 2 rows of vias (a) 8mm (b) 10mm and (c) 20mm	45
Figure 3.7	Varied value of flaring angle (a) 17° (b) 19° and (c) 22°	45
Figure 3.8	Varied value of distance between 2 vias (a) 2mm (b) 2.5mm and (c) 3mm	46
Figure 3.9	Varied configuration of both side horn antenna (a) 20mm gap (b) 20mm loading and (c) no loading	48
Figure 3.10	Finalize design of SIW sensor	48
Figure 4.1	Simulated scattering parameter for basic design from [29]	51

Figure 4.2	Simulated scattering parameter for basic design from Shibu [30]	51
Figure 4.3	Simulated reflection coefficient for horn antenna design from [29]	52
Figure 4.4	Radiation pattern result (a) Tavin [29] (b) simulated	53
Figure 4.5	Simulated reflection coefficient for horn antenna design from [30]	53
Figure 4.6	Radiation pattern result (a) Shibu [30] (b) simulated	53
Figure 4.7	Simulated reflection coefficient for varied 'a' value from 8mm, 10mm and 20mm	54
Figure 4.8	Simulated reflection coefficient for varied angle from 17°,19° and 22°.	55
Figure 4.9	Simulated reflection coefficient for varied pitch from 1mm, 2mm and 3mm	56
Figure 4.10	Simulated scattering parameter for configuration with 20mm gap	57
Figure 4.11	Simulated scattering parameter for configuration with 20mm loading	57
Figure 4.12	Simulated scattering parameter for configuration with no loading	58
Figure 4.13	Simulated scattering parameter for finalize design	58
Figure 4.14	Radiation pattern in (a) 3D and (b) polar for finalize design at 5GHz	59
Figure 4.15	Simulated (dashed line) and measured (solid line) reflection coefficient for finalize design	59

LIST OF ABBREVIATIONS

SIW	Substrate Integrated Waveguide
CST	Computer Simulation Technology
S-Parameter	Scattering Parameter
MUT	Material Under Test
VNA	Vector Network Analyzer
UWB	Ultra-Wide Frequency Region
CVAAS	Cold-vapour Atomic Absorption Spectrometry
PCR	Polymerase Chain Reaction
MIMO	Multiple Input Multiple Output
TE	Transverse Electric
PCB	Printed Circuit Board
RF	Radio Frequency
SINRD	Substrate Integrated Non-Radiative Dielectric
SIINDG	Substrate Integrated Inset Dielectric Guide
SUT	Sample On Test
TRL	Through-Reflect-Line
VSWR	Voltage Standing Wave Ratio

CHAPTER 1

INTRODUCTION

1.1 Project Background

Microwave technology is rapidly advancing in its capacity to determine complex permittivity and permeability properties of materials [1]. These permittivity characteristics can be calculated in a variety of methods. Nonetheless, a straightforward and low-cost method for determining complex permittivity in the millimetre wave and microwave frequency ranges is required.

The theoretical concepts and practical components involved in determining a substance's dielectric characteristics via the interaction of electromagnetic fields with it are interrelated. These fields must then be created, directed, or radiated over the sample (MUT - material under test), and detected.

There are two types of methods: resonant and non-resonant [3]. The material can be characterised using resonant methods at a single or many discrete frequency points. A dielectric material is utilised as a resonant element in this method, although it is only applicable to low loss test samples; examples include dielectric, planar, and split resonators.

Non-resonant techniques are ideal for broadband measurement. Changes in the characteristic impedance and wave velocity result in changes in the reflection and transmission coefficients of the material, which may be used to classify it. The transmission line (waveguide) method, the free space method, the resonant cavity method, and the coaxial probe method are only a few of the most widely used and critical approaches for dielectric measurements.

The resonant approaches are insufficient for frequency domain characterization. Spectroscopy can be performed using reflection techniques, also known as single-port

techniques, are used to determine the reflection coefficient of a guided wave or a free-space wave. The free space technique is particularly well adapted to measuring dielectric constants because of its non-destructive properties and non-contact [4].

1.2 Problem Statement

Various methods have been used for material characterization. However, these methods have issues that are specific to their uses. For instance, techniques that require vacuum cannot be used for analysing liquid or volatile chemicals. This limitation means that a given technique may have a limited range of applications. As a result, the SIW sensor is suggested as an option for developing a sensor since microwave technology has high sensitivity detection and measurement accuracy. Another issue is the need to submit the sample to a specific laboratory for analysis, which takes longer. This innovative alternative material has the potential to replace the commonly utilized dielectric substance in electrical equipment using a sensitive sensor that can define the material while maintaining the product non-destructive and clean, as well as user-friendly and time-saving.

1.3 Objective

Many methodologies and hundreds of papers have been published reporting a wide variety of methods for determining the dissipation factor and dielectric constant of the dielectric materials.

The objective of this research is modelling the Substrate Integrated Waveguide (SIW) sensor capable of characterizing materials by using engineering computational tools.

Next, analysing the performance parameter in a certain frequency using Computer Simulation Technology (CST) Studio to determine the appropriate parameter value for the SIW model in term of dimensions and materials so it is possible to minimize sensing time and enhance accuracy in extracting dielectric characteristics of materials.

Lastly, evaluating the performance parameter by performed measurements on a fabricated prototype model to validate the simulation performance result.

1.4 Scope of the project

SIW sensor will be designed using Polylactic Acid (PLA) through CST software and the scattering parameter should be under -10dB at G-band (4-6GHz) using Horn Antenna principle.

1.5 Summary

Thesis organization is as follow:

The first chapter of the project contains the thesis introduction, which includes the context of the project, the problem description, the project objectives, and the project scopes.

The second chapter is dedicated to a literature review. It mostly consists of a detailed explanation of the project's concept. It also includes an assessment of a number of initiatives completed by researchers from other universities. As a result, the results of these initiatives can be compared to those of others, and the differences can be seen more clearly. In Chapter 2, previous work on transitions between SIW and SIW horn antennas is discussed.

The methodology is covered in Chapter Three. It comes with a flowchart that shows how the project was completed. The approaches in this thesis are started with reproduce previous develop design research, then continue with basic structure before the transition to horn antenna structure. In addition, the CST software was used to simulate the SIW sensor.

The results and discussions are presented in Chapter Four. It will include all of the outcomes of the project's analysis and design, including the project's progress. The findings of the simulation, as well as the design, are presented and analysed.

In Chapter 5, the conclusion will be discussed. The conclusion has been reached, and recommendations have been given for future work. The recommendation is included to express an opinion as well as a suggestion for how future work should be done.

CHAPTER 2

LITERATURE REVIEW

2.1 Introduction

This chapter provides the fundamental theory of SIW as a one of the topologies of SIC. The SIW technology has been well applied to several millimetre-wave and microwave components. The structures of SIW, the available model of SIW and the important parameters are also discussed in this chapter.

2.2 Dielectric properties

Permittivity is a charge attribute that determines how quickly charges may align (polarise) in the appearance of an electric field [5]. Increased permittivity suggests that the creation of an electric field is less difficult and that disturbances propagate more slowly through the medium.

The oscillation frequency is unaffected by a high-permittivity material surrounded by a low-permittivity material; however, the high-permittivity material slows wave propagation. If we remember from Equation 2.1 that wave speed equals the frequency and wavelength relationship, we can see that a drop in speed must be followed by a decrease in wavelength if frequency remains constant.

The speed and wavelength of a wave increase when it exits a material with a high permittivity.

$$c = f\lambda = 3.0 \times 10^8 \text{ m/s} \quad 2.1$$

$$\kappa = \epsilon_r = \frac{\epsilon_m}{\epsilon_0} \quad 2.2$$

$$\lambda_0 = \frac{c_0}{f} \text{ (free space)} \quad 2.3$$

$$\lambda = \frac{c_0}{f \sqrt{\epsilon_r}} \text{ (dielectric)} \quad 2.4$$

In equation 2.2, ϵ_r denotes relative permittivity, which is defined as the ratio of the material's permittivity to the permittivity of vacuum. When an antenna is enclosed in a material with a high permittivity, the size of the antenna may be lowered to match the shorter wavelength of electromagnetic waves in its near nearby [2]. According to equations 2.3 and 2.4, there is a difference in wavelength while in empty space or when utilising a dielectric.

Magnetic permeability refers to a material's capacity to store energy in magnetic fields. Bear in mind that antennas transmit electromagnetic radiation, which consists of both electric and magnetic forces. As a consequence, permeability, like permittivity, has an effect on the propagation of electromagnetic waves. Permittivity and permeability both contribute to the reduction of wave velocity and the lengthening of wavelengths.

$$\mu_r = \frac{\mu}{\mu_0} \quad 2.5$$

The relative permeability is described in equation 2.5 as the ratio of a substance's permeability to the permeability of a vacuum [6]. Consider the "speed of light," which is really the speed of electromagnetic radiation in general, to emphasise the principle that permittivity and permeability affect the speed radiation of electromagnetic. The temperature coefficient of resonant frequency, as indicated in Table 2.1, characterises the frequency shift of dielectric materials produced by temperature change.

Table 2.1 The resonant frequency of various standard dielectric sample

Frequency	Material	Dielectric constant
0.33GHz [7]	Butanol	2.95
0.54GHz [7]	Propanol	3.2
8Ghz [8]	Silicon	11.69
10GHz [9]	Bakelite	3.7
10GHz [9]	Teflon	2.08

2.3 Measuring Technique for Characterization of Dielectric Materials

The study of dielectric characteristics is crucial for understanding the interaction of materials in the magnetic region. Knowing and understanding the dielectric characteristics of materials can help engineers design efficient and effective microwave heating methods and products. In this analysis, many enclosures wall materials' dielectric properties have been calculated using the coaxial sample process. Due to its simplicity and high precision, this approach was chosen. There was a similar activity in all materials.

Permittivity and permeability are frequency-dependent qualities, not constants. Conduction, dipolar relaxation, atomic polarisation, and electronic polarisation all play a role in determining the permittivity of a dielectric material [3]. At low frequencies, the influence of ion conductivity is prominent, but at microwave frequencies, dipolar relaxation is the predominant source of permittivity change. Infrared and above absorption peaks are mostly caused by electronic polarizations and atomic.

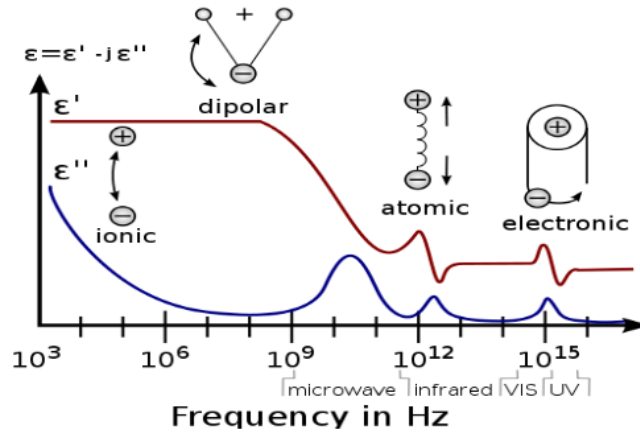


Figure 2.1 The frequency dependence of a hypothetical dielectric's permittivity. The frequency dependence of the permittivity of a hypothetical dielectric. In Figure 2.1, the permittivity of a hypothetical dielectric is displayed versus frequency up to a specific value. It diminishes at microwaves, with some peaks and variation above that, but only within a narrow range. Additional information on this diagram may be found in the literature. When an electric field displaces the intervening electrons relative to the nucleus, neutral atoms undergo electronic polarisation [5].

Atomic polarisation when an electric field is given to nearby positive and negative ions, they stretch. Certain sources may produce the relaxation phenomena, and the dielectric material possesses a relaxation-time continuum in certain situations. In a wet medium, for example, water molecules are bonded with variable degrees of strength. The material shows a distribution of relaxation frequencies based on the frequency of the binding water and the moisture content.

The measuring fixture is called a coaxial dielectric probe. This approach is wide, straightforward, and handy (non-destructive), but it is imprecise and works best with liquids or semi-solids. To provide proper capacitance and reproducibility of sample loading, the probe is often put into a flange. The open-ended coaxial probe is a severed section of transmission cable. Submerging the probe in liquid or pressing it to the flat face of a solid allows the material to be weighed (or powder).

When there is contact made between fields at the probe end and the specimen, they "fringe" and move into the sample [10]. This approach assumes that the sample is not magnetic, isotropic, homogeneous, and, if it is a solid, has a flat surface. The sample should be sufficiently thick, "semi-infinite," and much larger than the diameter of the opening of the open-ended coaxial line, since this approach requires no interaction between the electromagnetic field and the sample's non-contacting boundaries.



Figure 2.2 A coaxial probe with flange.

Between the probe and the sample, there must be no air spaces. In comparison to other methods such as the coaxial line reflection, transmission line and resonator reflection, this technique has a lower accuracy under certain situations.

Following that, the free space approach is a non-destructive and contactless technique for characterising and quantifying the characteristics of dielectric materials [3]. It has found use in the characterisation of solids, particularly those operating at high temperatures and requiring minimum handling. While it is unusual, it has been used in a few published studies to characterise liquids.

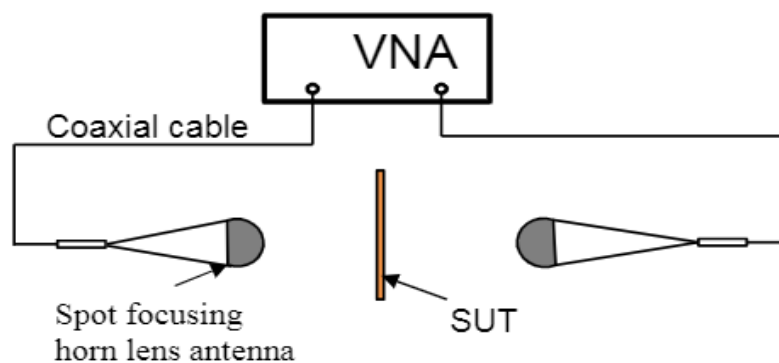


Figure 2.3 Illustration of free space method for material characterization

As with transmission and reflection, a liquid as an SUT must be enclosed in a dielectric with established electrical characteristics. The sample will subsequently be separated into three pieces, as indicated in Fig. 2.10: dielectric with known characteristics, SUT, and dielectric with known properties.

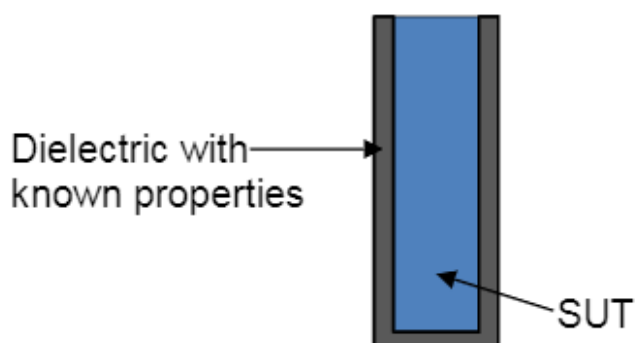


Figure 2.4 Illustration of an encapsulation for the purpose of determining the properties of a free space liquid

In this case, the free-space wave impedance serves as the line Z_0 characteristic impedance. The free space technique spans a broad range of wavelengths, from microwave to millimetre, and hence enables the characterisation of a large variety of materials. Numerous variables affect the accuracy of the free space approach, including ensuring that the antenna emits a plane electromagnetic wave onto a central plane and that the wave passes through the SUT with little diffraction [3]. Due to these two concerns, as well as the need for a safe environment surrounding the measurement equipment, this technique may be hard at times.

The through-reflect-line (TRL) is widely used for calibration. The antennas must be positioned towards the start of the far sector, which is $2D/2$, during the initial setup. Where is the horn antenna's enormous diameter? As previously stated, the primary selling point of this technology is that it offers a fully contactless way of measuring [4]. Regardless of its exact limitations, the requirement of contactless measurement in some applications may make it the technique of choice. As previously stated, such applications include the assessment of harmful compounds or heated samples.

Parallel plate

A dielectric substance is sandwiched between two electrodes to generate a capacitor in the parallel plate capacitor method. As shown in Figure 2.5, measurements can be made with an LCR metre or impedance analyser and a dielectric fixture [3]. However, if the air gap and its consequences are not evaluated and calibrated, they might create significant mistake.

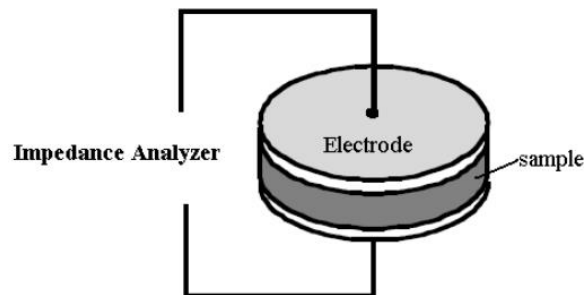


Figure 2.5 Parallel Plate illustration method

Resonant cavities

This technique is often used for dielectric measurements of homogeneous materials because to its simplicity, increased accuracy, and support for high temperature measurements. Additionally, it provides accurate results for materials with low dielectric loss and a low loss factor.

When a sample is placed into the waveguide's centre, whether circular or rectangular, the centre resonant frequency and quality factor change, revealing information about the inserted sample and allowing for the calculation of the dielectric constant [6].

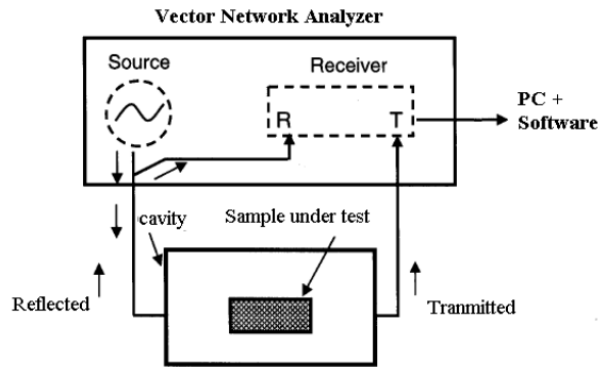


Figure 2.6 Cavity resonator method illustration

Transmission line

Another common technique, as seen in Figure 2.7, is to place a material sample in the centre of an enclosed transmission line. Both coefficients are used to determine the amount of light reflected and transmitted. It is more precise and sensitive than coaxial lines, but has a smaller frequency range.

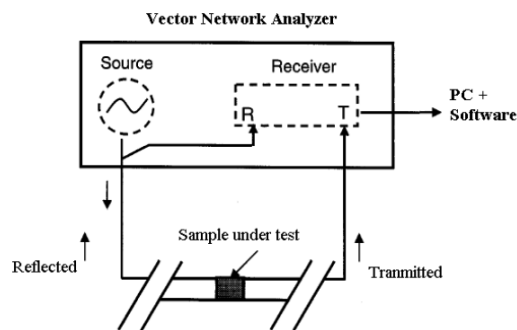


Figure 2: Transmission Line (Waveguide) Method [8]

Figure 2.7 Transmission line (waveguide) method illustration

Table 2.2 provides a general comparison of techniques. The coaxial probe technique can operate over a large frequency range, however due to the metallic probe, it requires periodic calibrations, and air gaps might cause some mistakes. While the free space technique is applicable to non-contact testing, the disadvantage is that the low end is constrained by a reasonable sample size [3-4].

Parallel plate capacitors are a low-frequency, somewhat accurate approach for measuring high-loss materials. It works effectively with thin, flat-surfaced samples. The most precise technique is a resonant cavity that accommodates both liquid and solid samples, but it is restricted to low-loss and very small samples. Electric and magnetic characteristics of solid and liquid samples may be determined using the transmission line (waveguide) approach.

Table 2.2 Comparison of characterization technique

Method of characterizations	Advantages
Coaxial probe	A metallic probe is used to detect reflected signals. Broad frequency range around 0.5GHz to 110GHz
Free space	VNA was used to direct radiation through material placed between two horn antennas. No physical contact
Parallel plate	Placing a dielectric sample in a sample holder and determining permittivity based on the capacitance value. Low frequencies are used; below 1GHz
Resonant cavities	The sample is positioned in the waveguide's centre, resulting in changes in the waveguide's centre resonant frequency and quality factor. Typical measurement range is 50MHz to more than 100GHz.

Transmission line (waveguide)	<p>Inside the enclosed transmission line, a material sample is placed.</p> <p>Its frequency range is smaller than that of coaxial.</p>
----------------------------------	--

2.4 Substrate Integrated Waveguide (SIW)

Both planar printed transmission lines and classic waveguides face the same integration difficulty when designing a full RF system. Due to the fact that active, passive, and transmission components are often constructed using distinct techniques and interfaces, extra losses occur during insertion, transfer, and transmission operations. As a result, it is impossible to get the best feasible design output for each device component [11]. In order to optimise system integration, an unique guided structure known as the substrate integrated waveguide (SIW) has been designed, as depicted in Figure 2.8 (a). Furthermore, the transmission lines manufactured by the SIW not only have planar printed transmission line physical features, but they also have solid waveguide output.

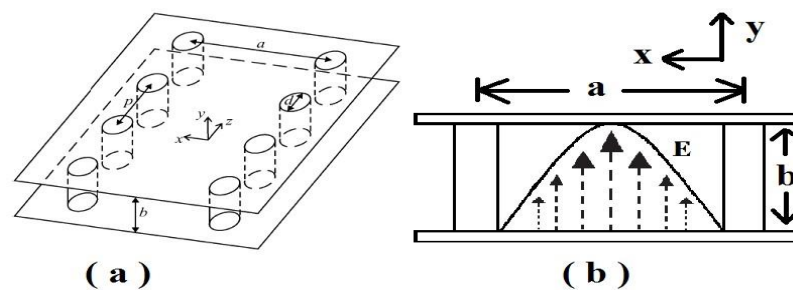


Figure 2.8 (a) SIW perspective view structure; (b) SIW basic mode in cross-section view

SIW is constructed similarly to a rectangular dielectric-filled waveguide. SIW, on the other hand, reduces the initial height to the PCB thickness using the Microstrip PCB manufacturing technology. In this case, the PCB substrate may be considered as the waveguide's inner-filled dielectric. The two waveguides' metallic broad sides are similar to the two copper PCB sheets [11-12]. Two rows of electroplated through holes are bored into the PCB to replace the waveguide's thin walls. As a consequence, the copper

sheets and through holes form a current loop in cross-section, comparable to the cross-section of a standard solid metal waveguide. Additionally, each of these through holes is drilled at the same distance and time.

By being reflected, the compressed electromagnetic wave in SIW goes forward via a zigzag route between the two rows of through holes, similar to how bulky waveguide propagates. As a result, each SIW's lowest transmission frequency is distinct. Furthermore, the wavelength of the cut-off frequency should be proportionate to the SIW distance. Due to the thinness of the PCB, SIW's height "b" is usually less than 2 mm [13]. The through hole configuration is also dense, suggesting that the gap "p" between two posts, as well as the post diameter "d," is small.

As a result, SIW suffers from extremely minimal attenuation and loss. SIW's biggest distinctive feature is the current distribution on through holes. The surface current in a standard waveguide can flow in any direction.

2.4.1 SIW Mechanism

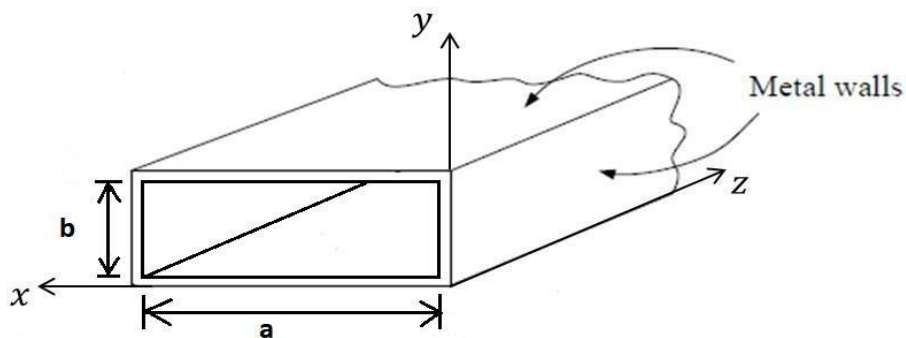


Figure 2.9 Rectangular waveguide structure

The letters "a" and "b" denote the width and height of the rectangular waveguide dimension, respectively, as shown in Figure 2.9. In general, the breadth should be bigger than the height [13]. The cross-section of a waveguide at any junction is displayed in an x-y plane. The length of the waveguide is measured along the z axis. The hollow space in the centre waveguide can be filled with dielectric material. Metal walls surround the

waveguide on all sides. After being reflected on the metal's inner surface, the electromagnetic wave within the waveguide propagates in a zigzag pattern. Electromagnetic waves can only go in one direction: in the direction of the z axis.

The transverse electric (TE) mode, shown in Figure 2.10, is the most frequent mode of propagation in rectangular waveguides. It is characterised by all electric field components being perpendicular to the propagation direction. The first TE mode, as seen in Figure 2.10, is TE₁₀. In this mode, only the electric field components along the y-axis direction change. Vertical solid lines in the x-y plane depict the y axis's E-field components. The waveguide's dash loops depict the magnetic field. The crosses denote components of the E-field pointing downhill, while the dots indicate components of the E-field pointing upward [14].

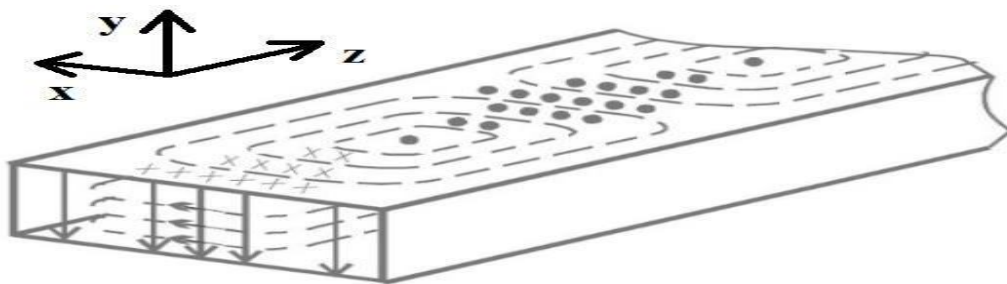


Figure 2.10 Electromagnetic field distribution of TE mode.

Lord Rayleigh was the first to develop an inner conducting hollow pipe prototype by solving the mathematical boundary issue and identifying the transmission mode, according to the oldest official record of waveguide. Most frequency bands employed in laboratories at the time were below the bulky tube's cut-off frequency due to the unavailability of a high-frequency source actuator.

As a result, tests based on this theory failed to confirm the directed tube assumption's validity. And the assumption was placed on the back burner. Barrow and South worth, two American scientists, did not obtain experimental proof for waveguide feasibility until 1936 [15]. Later on, the Bell telephone research group carried out the

mathematical proof of waveguide. Since then, a growing number of research papers have shown that the metallic hollow pipe can be used as an antenna radiator as well as an enclosed electromagnetic wave transmission line. Detailed waveguide property and characteristic analysis was accomplished in the 1940s. Watson's work on the resonant slot of a rectangular waveguide, in particular, has had a major impact on the waveguide formula derivation. Since the 1950s, the tried-and-true formula has been commonly applied to waveguide structures made with various fabrication technologies.

2.4.2 Design Guidelines

The following are the stages to designing a SIW horn with the specified shifting:

1. The horn dimensions (D, W, and a) are determined with a particular substrate (h) to excite just the TE₁₀ mode and yield error of a quadratic phase at the horn aperture that is acceptable.
2. The number of blocks (N) is proportional to the number of needed frequency bands. Equations 2.6 and 2.7 are then used to get the beginning dimensions of the printed transition (L and s).

$$fr_1 = \frac{c}{2L_{eq}\sqrt{\epsilon_r}} \quad 2.6$$

$$fr_2 = \frac{fr_1}{\sqrt{1 \mp k_2}} \quad 2.7$$

However, when determining the values of L, s, h, and, the following tendencies should be kept in mind:

First, boosting the h/L ratio improves matching and bandwidth, but it may also excite other modes. Next, lowering the s/L ratio reduces radiation losses while simultaneously lowering bandwidth. Additionally, increasing the value of raises the antenna-air mismatch even more.

The following is a suitable trade-off: 0.25 h/L 0.5, 0.03 s/L 0.06, 5. When the transition dimensions are within these parameters, the two suggested models are very accurate.

When selecting the number of blocks, it is not recommended to use more than three. Increased radiation losses result in narrower and poorer resonances as the number of blocks grows. [16]

2.5 Different Model of SIW from Previous Research

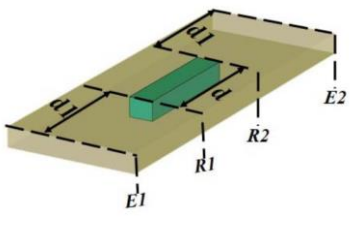
There are many sensor examples based on substrate integrated waveguide technology for characterization of dielectric material. Dielectric measurements are performed on a variety of solid, liquid, and powder samples [17-19].

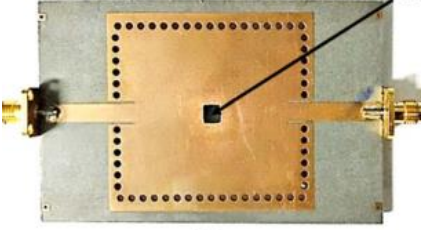

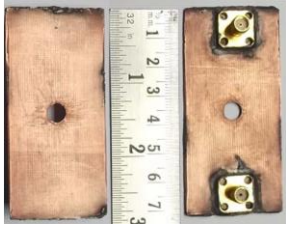
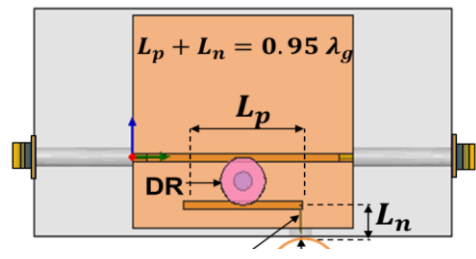
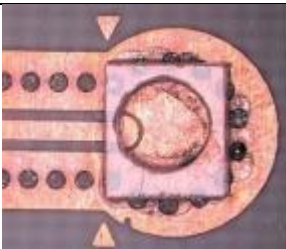
2.5.1 Model for Material Detection

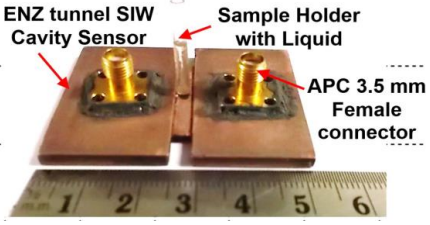

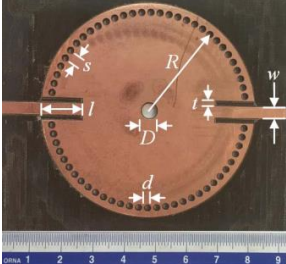
Main material commonly can be characterize using SIW sensor is solid, powder and liquid. In Table 2.3, comparison between the sensor design based on the material detected is presented. Both sensors have a special slot drilled at the location of the electric field maxima for inserting the solid detection test samples.

While for powder, the model is consisting of array of holes at the center of the SIW sensor. Most of the SIW sensor for liquid detection have sample slot like solid detection sensor but a cylindrical cavity in a small glass container placed for sample holder, or the SIW sensor is immersed in the liquid itself for detection purpose.

Table 2.3 Solid, powder and liquid detection with its antenna type used and working frequency

Material detection	Sensor design	Antenna type	Frequency range (GHz)
Solid	 <p>[17]</p>	Partially filled SIW	8-12GHz

	 <p>[18]</p>	SIW cavity sensor	6.5GHz
Powder	 <p>[19]</p>	SIW resonator sensor	2.5GHz
Liquid	 <p>[20]</p>	SIW cavity sensor	2.4GHz
	 <p>[21]</p>	SIW resonator sensor	5.72GHz
	 <p>[22]</p>	Impedance sensor	12GHz

 <p>ENZ tunnel SIW Cavity Sensor</p> <p>Sample Holder with Liquid</p> <p>APC 3.5 mm Female connector</p> <p>[23]</p>	SIW cavity sensor	0.8-19MHz
 <p>[24]</p>	HM-SIW resonator sensor	5-6GHz
 <p>[25]</p>	SIW cavity sensor	2.45GHz

The structure comprises of a rectangular SIW waveguide and a tapered waveguide that facilitates the propagation of the basic mode TE₁₀ of SIW structures with a radiating aperture length of d_1 .

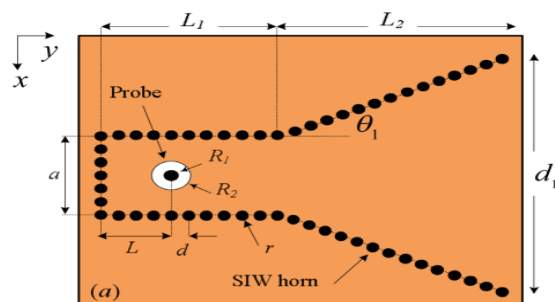


Figure 2.11 Structure of conventional SIW Horn

Figure 2.16 shows the structure of the conventional SIW horn, which is made up of one rectangular and two tapered portions. L_1 and L_2 are the lengths of the various tapered portions, with angles of θ with regard to the horizontal line, respectively [26]. are

selected in such a way that both horns have the same diameter radiating aperture. They are connected through a fifty-ohm coaxial cable with the inner radius of R1 and the outer radius of R2. To prevent spurious radiation generated by the gap between adjacent vias, the radius and the distance d between adjacent vias of each are chosen using the defined principles. The angle of the first half of both horn antennas is set to maximise gain in accordance with the intended guideline for conventional horns. As a consequence, SLL and backward radiation are decreased, while the antenna gain increases. Additionally, a grounded pin is put in the aperture's centre to improve the antenna gain even more.

2.6 Important Sensor Performance Parameter

To determine the fields radiated by the horn, just the tangential components of the E- and/or H-fields over a closed surface must be known. The closed surface is intended to resemble an infinite plane that goes through the mouth of the horn. When the flare is prolonged beyond that point, the flatness (with a certain amount of allowable ripple) increases, and the major maximum eventually returns to the axis. It's also worth noticing that as the flaring grows, the pattern's cut-off characteristics become substantially sharper. [15]

In practise, a lens is typically placed at the aperture to compensate for the phase taper at the opening, which invariably results in a smaller pattern as the horn flares. When the horn length is varied while keeping the flare angle fixed, similar pattern changes occur. As the length expands, the design becomes more rounded, finally becoming flatter (with a ripple). Beyond a certain length, the primary maximum does not occur on axis, and the pattern continues to expand and flatten (within an allowed ripple) until the maximum returns to axis. The method is infinitely repeatable.

2.6.1 Scattering Parameter

S-Parameters is introduction to electrical networks with matched impedances are characterised using S (scattering) characteristics. When travelling currents or voltages reach a discontinuity in a transmission line, the term "scattering" refers to how they are affected. S-parameters allow a device to be viewed as a "black box" with inputs and outputs, allowing a system to be modelled without having to deal with the intricate details of its structure [27].

The concepts of high-frequency model verification can be demonstrated with a simple RF relay. An RF relay is a three-port device with an input, output, and a control to turn the circuit on and off, as shown in Figure 2.12. The relay can be simplified to a two-port device if the device's performance is independent of the control terminal once configured. As a result, examining the behaviour at the device's input and output terminals can provide a complete picture of the device.

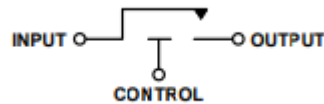


Figure 2.12 RF relay model

Assume the transmission line has two ports, as indicated in Figure 2.12. Every moving wave is made up of two components, as can be seen in this diagram. The total travelling wave component flowing from the two-port device's output to the load, b_2 , is really made up of the fraction of a_2 that is reflected from the device's output plus the amount of a_1 that is transmitted via the device [28]. In contrast, the total travelling waves flowing from the device's input back toward the source, b_1 , are made up of the reflected component of a_1 plus the proportion of a_2 that is transmitted back via the device.

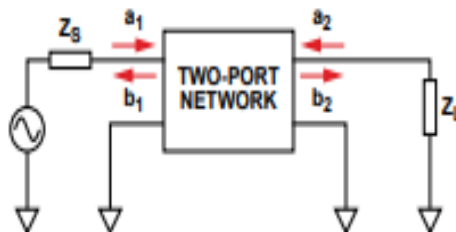


Figure 2.13 S-parameter model

Where, a_1 = Travelling wave incident on Port 1

b_1 = Travelling wave reflected from Port 1

a_2 = Travelling wave incident on Port 2 (Reflected from the load)

b_2 = Travelling wave reflected from Port 2

Equations using S-parameters may be built to determine the values of reflected waves using the given interpretations. The reflection and transmission wave equations are shown in Equations 2.1 and 2.2.

$$b_1 = S_{11}a_1 + S_{12}a_2 \quad 2.8$$

$$b_2 = S_{21}a_1 + S_{22}a_2 \quad 2.9$$

When Z_S equals Z_0 (the impedance of the two-port input), there are no reflections and a_1 equals 0. When Z_L equals Z_0 (the impedance of the two-port output), there are no reflections and a_2 equals 0. As a result, we can define the S-parameters as follows:

$$S_{11} = \frac{b_1}{a_1} \quad 2.10$$

$$S_{21} = \frac{b_2}{a_1} \quad 2.11$$

$$S_{22} = \frac{b_2}{a_2} \quad 2.12$$

$$S_{12} = \frac{b_1}{a_2} \quad 2.13$$

Where S_{11} denotes the input reflection coefficient, S_{12} denotes the reverse transmission coefficient, S_{21} denotes the forward transmission coefficient, and S_{22} denotes the reverse reflection coefficient in the preceding equations 2.3, 2.4, 2.5, and 2.6.

Any two-port system can be completely represented by these equations, with S_{21} and S_{12} denoting forward and reverse gain, and S_{11} and S_{22} denoting forward and reverse reflected power. Z_S , Z_0 , and Z_L must be matched in order to implement the above parameters in a physical system. For the majority of systems, this is a straightforward implementation over a broad frequency range.

2.6.2 Directivity

One of the metrics that is frequently used as a figure of merit to define an antenna's performance is its directivity. The maximum radiation is created to determine the directivity. The directivity of an antenna system is frequently used to assess its overall performance. An electrically small antenna produces low directivity, according to the general rule in antenna theory [10]. That is, if you utilise a directivity antenna with a total size of 0.25 - 0.5 wavelength, you will have the least amount of directivity (a quarter- to a half-wavelength in size). Half-wave dipole and half-wavelength slot antennas, for example, generally have directivities of less than 3 dB, which is about as low as it gets.

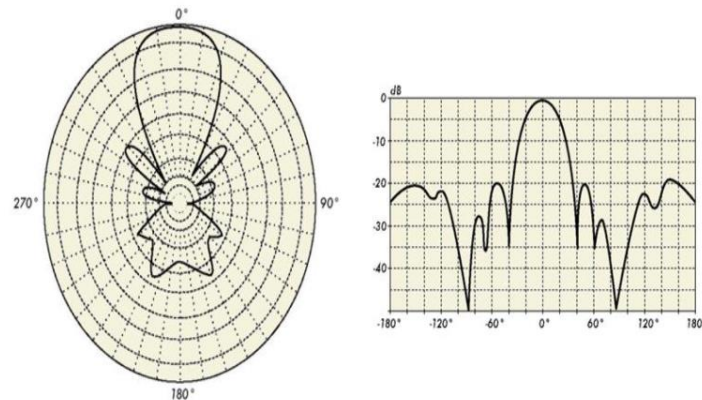


Figure 2.14 Far-field radiation patterns

Due to the complexity of the antenna, only one contour (isoline or isosurface) is used to depict far-field radiation patterns. The contour lines and contour surfaces are centred on orthogonal planes that overlap the antenna, usually around a line of symmetry. The Hertzian dipole seen above transfers relatively little, if any, energy upward.

CHAPTER 3

RESEARCH METHODOLOGY

3.1 Introduction

This chapter will be discussed on construction of basic and horn antenna SIW sensor structure based on literature review and manipulate the geometrical parameter to execute the finalize SIW sensor.

3.2 Flowchart

In this thesis, the modelling procedure is followed:

First step for the modelling phase is to reproduce basic SIW design from a selected research paper or article. From the literature review, we choose two (2) research papers to reproduce the design with parameters provided. The simulation is done using CST software and the performance observed is S-Parameter and radiation pattern. If the performance obtained is close to the provided results in the paper, we achieve the target and will repeat the basic design process if vice versa. When the first target is achieved, we continue to the next step which is to reproduce SIW horn antenna structure from a research paper or article. From the literature review, we select also two (2) research papers to reproduce the design with the parameters provided. If the performance obtained is close to the provided results in the paper, we achieve the target and will repeat the basic design process if vice versa. Once the second target is achieved, the modelling phase is verified and continue to the analysis phase.

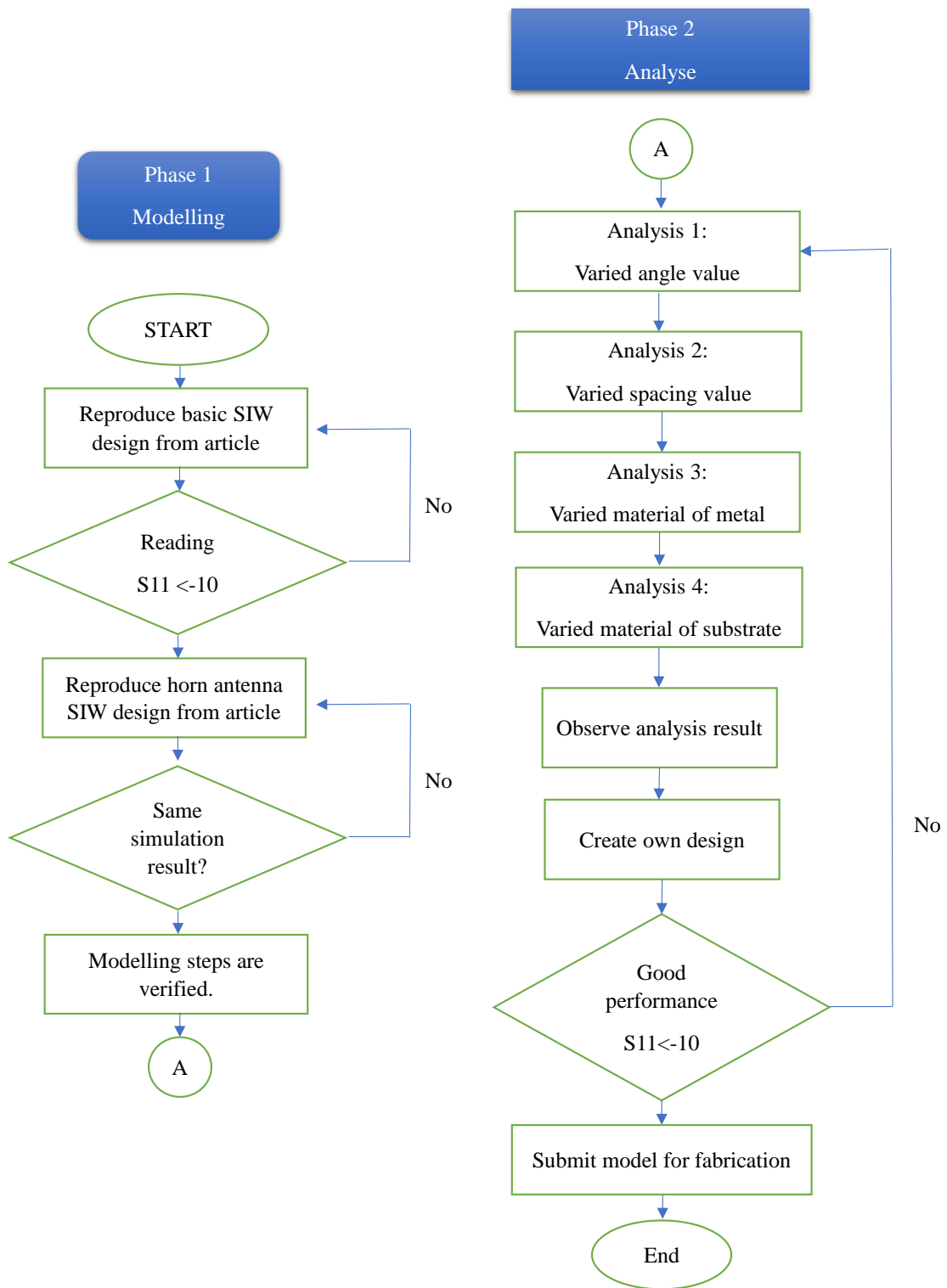


Figure 3.1 Overall flowchart for modelling SIW and analyse the geometrical parameter of SIW sensor

The analysis starts from varied the parameters such as angle value and spacing value, also varied the material of metal and substrate to observe the performance. The performance when increment and decrement of parameters values, and the changes of materials are observed. These four (4) analyses are done using both basic and horn antenna structure. The performance is considered good if the S-parameter is below -10dB.

3.3 Numerical result

The SIW Horn Antenna's designation, as well as the size and positioning of via holes, are critical. The three characteristics of via holes are the diameter (d), the spacing between adjacent vias (s), and the distance between the two rows of via holes (a). According to SIW theory, the ratio of spacing to diameter will be equal to or less than 2.

The SIW will be made up of substrates that are 1.7mm thick. The diameter of a via hole cannot be smaller than the thickness of the substrate due to fabrication constraints. The diameter of the via holes is set to 1.5mm, as per the instructions. The spacing to diameter ratio will be two millimetres.

The chosen dimensions of $d=1.5\text{mm}$ and $s=2\text{mm}$ will ensure that leakage between the posts is kept to a minimum and has no effect on the SIW's performance..

After determining the size and spacing of the metallic posts, the distance between the two rows of via holes (a) must be calculated. This parameter has the same effect as a rectangular waveguide's width. The significance of (a) determining the cut-off frequencies of various modes that may exist in the SIW. The objective is to select (a) so that the SIW has the same properties as a rectangular waveguide with a width of 14mm. \

3.4 Consideration and design steps

The SIW is a rectangular waveguide-like device that may be synthesised and fabricated by inserting two rows of conducting cylinders, vias, or slots in a dielectric substrate sandwiched between two parallel metal plates.

Determining the cut-off frequency and effective width is a crucial step in SIW design. These formulas make it simple to calculate them;

$$f_c = \frac{m}{2a_{eq}\sqrt{\mu\epsilon}} \quad 3.1$$

$$W_{eff} = w - \frac{d^2}{0.95s} \quad 3.2$$

The width of the metallic waveguide and the dielectric constant inside the waveguide are both essential characteristics, as shown by this equation. When these two equations are referred to, these equations are very correct when;

$$\frac{d}{w} < 2 \quad 3.3$$

When choosing a substrate, there is always a trade-off between performance and cost. Conductor losses, dielectric losses, and radiation are the three main causes of SIW losses. Conductor losses are influenced by the metal used (usually copper), the roughness of the metal, and the height of the SIW. The first two cannot be controlled directly by the designer since they are reliant on the copper lamination quality of the substrate.

Based on the frequency and skin depth, the thickness of the metallization should be calculated accordingly. The thicker the substrate, on the other hand, the lower the losses, therefore there is a trade-off between losses and final device size and weight, especially with multi-layer PCBs.

There are minimal radiation losses when the diameter of the vias is high enough and the spacing between them is tight enough. An empirical formula may be used to compute the through spacing based on the diameter.

$$\frac{s}{d} < 2.5 \quad 3.4$$

Radiation leakage is caused by the gaps between metalized vias and slots. In order to ensure that the synthesised waveguide section becomes radiation less or leakage loss free, the parametric effects of p and d on those problems were examined. Dielectric and

conductor losses aren't considered since they complicate the analysis; the loss is solely due to radiation. It was determined that the diameter of the hole must fulfil certain geometric limitations in order to decrease return and leakage losses:

$$d < \frac{\lambda_g}{5} \quad 3.5$$

$$p \leq 2d \quad 3.6$$

Horns have a lot of gain, a wide frequency range, and are quite simple to make. Rectangular horns can be classified into three groups. Rectangular horns are well-suited to rectangular waveguide feeders. The horn is used to transition electromagnetic waves between waveguide and free-space modes. Knowledge of the fields over the aperture is used to determine the fields over the aperture of aperture antennas such as slots, open-ended waveguides, horns, reflectors, and lens antennas.

The principles of design are similar to those of a conventional horn. For each length, there is an optimal aperture that delivers the highest gain. The gain improvement becomes less and less substantial when the duration is extended. For an extremely thin substrate thickness in respect to propagation wavelength, electromagnetic waves will be confined within the substrate rather than propagating. The bandwidth diminishes as the mismatch between the SIW horn and the air grows.

3.5 Modelling of SIW Sensor

The reproducible result is a wider definition of replicability. This indicates that just because an experiment is reproducible does not guarantee it is replicable, because we can reproduce the results using different methods as long as the outcomes are the same.

The primary motivation for replicating a design from a reference publication is to increase the number of opportunities for new insights. Because we vary the experiment, we not only find different approaches to get the same results, but we also notice options that we may not have considered before. The next step is to double-check that everything was done correctly and to boost reliability, which leads to frequent practise to create reproducible data and evaluate the outcomes.

Due to the nature of science, we cannot be certain that the outcomes of research investigations and experiments are correct or will remain correct. It assists others to understand what was done when we were able to recreate the result.

In this thesis, we choose two (2) reference papers to reproduce the design and simulation result. Both of these papers provide the data which allows achieving the same results. The reporting on experiment performance, techniques and tools used allows us to fully understand the steps authors took to achieve the results provided.

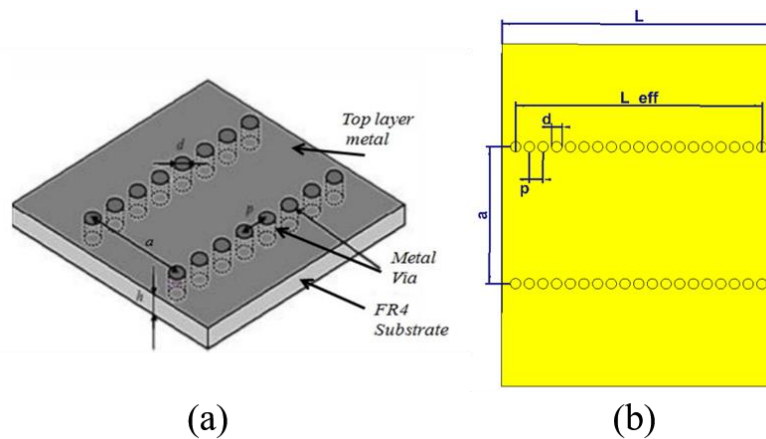


Figure 3.2 (a) Design and (b) reproduce design of SIW basic structure from Tanvi [29]

Based on paper reported by Tanvi [29], the basic SIW model are using FR4 with permittivity of 4.4 as substrate, with a thickness of 1.624mm.

Table 3.1 Parameter of the SIW basic structure for Figure 3.2

Parameter	Value (mm)
Diameter, d	1.5
Pitch (distance between 2 vias), p	2
Distance between 2 rows of vias, a	20
Total height, W	50
Total length, L	40

Total width (thickness), z_s	1.624
--------------------------------	-------

The substrate used for the design as shown in Figure 3.3 is FR4. A basic structure of this SIW sensor provides several characteristics, including the distance between two vias ('p'), the diameter of vias 'd', the distance between rows of vias 'a' and thickness of substrate are stated in detail in Table 3.2.

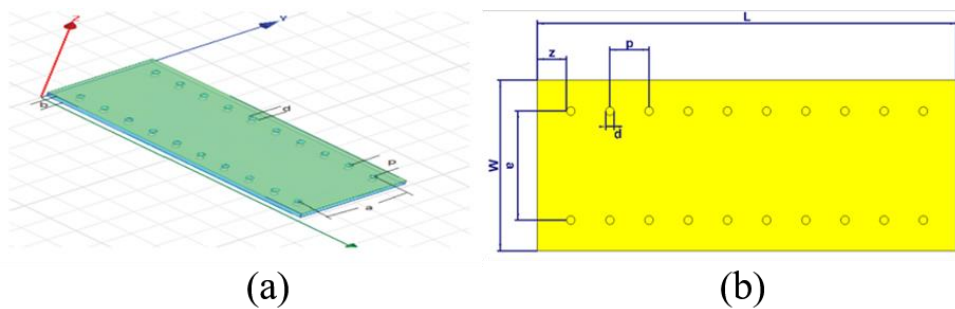


Figure 3.3 (a) Design and (b) reproduce design of SIW basic structure from Shibu [30]

Table 3.2 Parameter of the SIW basic structure for Figure 3.3

Parameter	Value (mm)
Diameter, d	1
Pitch (distance between 2 vias), p	4.7
Distance between 2 rows of vias, a	12.76
Total height, W	20
Total length, L	50.3
Total width (thickness), z_s	1.624

In the substrate integrated waveguide (SIW) technology, planar horn antennas are utilised to incorporate microwave and millimetre-wave electronics. The H-plane sectoral horn, which is created by flaring the rectangular waveguide in the plane normal to the electric field, may be created using SIW technology. Since then, the substrate integrated H-plane horn antenna has been published. Rectangular waveguide functionality may be incorporated into small planar devices using SIW (substrate integrated waveguide) technology.

As shown in Figure 3.7, a horn antenna has been developed utilising SIW technology, with L_1 being the length of the feed line and L_2 being the length of the flaring section. When excited with a waveguide port, this structure functions as a waveguide section, and the waveguide flaring generates.

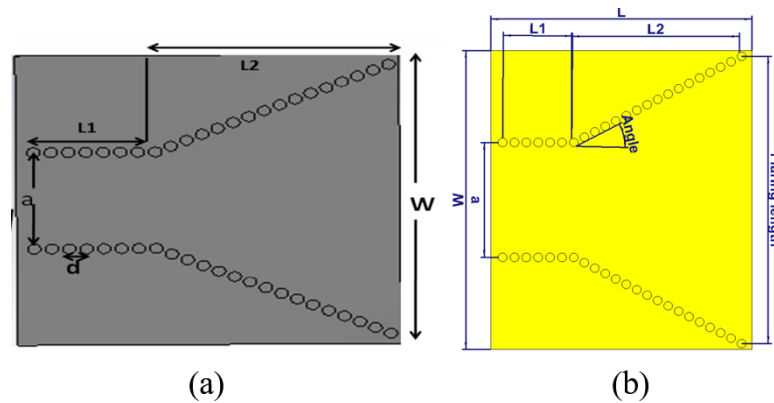


Figure 3.4 (a) Design and (b) reproduce design of SIW horn antenna structure from Tanvi [29]

The FR4 substrate, with a thickness of 1.624 mm with a relative permittivity of 4.4 and tangential loss of 0.004, has a relative permittivity of 4.4 and tangential loss of 0.004. With the requirements listed in Table 3.3, such as the center-to-center metallic vias distance 'p,' width 'a,' metallic vias diameter 'd,' and other factors.

Table 3.3 Parameter of the SIW horn antenna structure for Figure 3.4

Parameter	Value (mm)
Diameter, d	1.5

Pitch (distance between 2 vias), p	2
Distance between 2 rows of vias, a	20
Total height, W	52
L1	11
L2	28
Total length, L	44
Flaring length	50
Aperture angle	29°

The design in Figure 3.5 operates in the X-band, and Table 3.4 lists characteristics such as the horn's flare angle of 30.5 degrees, the aperture length of the horn antenna, and so on.

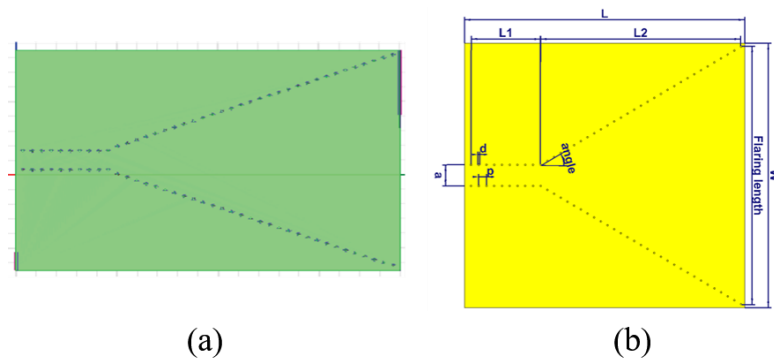


Figure 3.5 (a) Design and (b) reproduce design of SIW horn antenna structure from Shibu [30]

Shibu [30] computed each and every portion of the SIW to reformulate it to an X-band Horn Antenna, and the following structure was constructed using HFSS. Table 3.4 lists all of the parameters.

Table 3.4 Parameter of the SIW horn antenna structure for Figure 3.5

Parameter	Value (mm)
Diameter, d	1
Pitch (distance between 2 vias), p	4.7
Distance between 2 rows of vias, a	12.76
Total height, W	160
Length of the feed line, L1	42.05
Length of the flaring section, L2	121.49
Total length, L	170
Flaring length	156.39
Total width (thickness), zs	1.624
Aperture angle	30.5°

3.6 Analysis of Distance between 2 rows of vias of SIW sensor

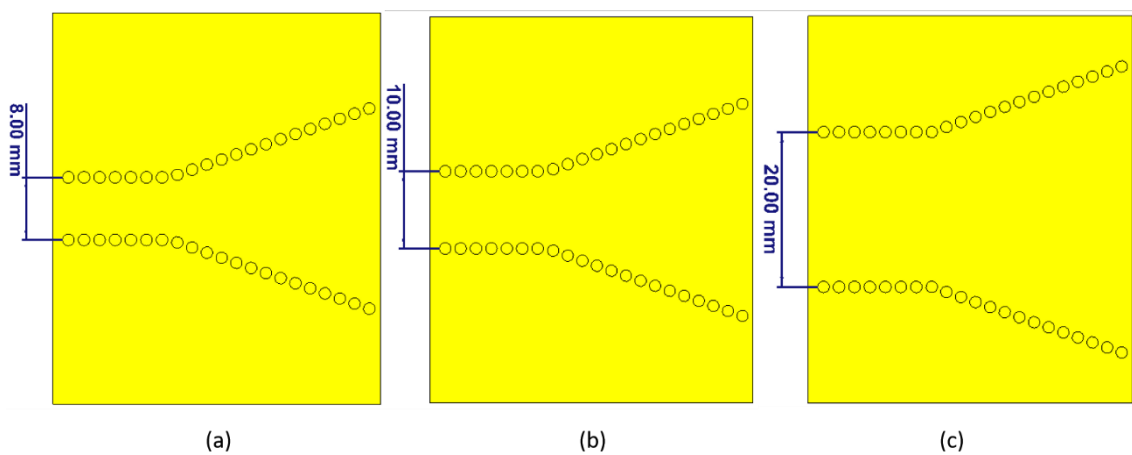


Figure 3.6 Varied value of distance between 2 rows of vias (a) 8mm (b) 10mm and (c) 20mm

Width is one of the main parameters of SIW where the distance between 2 rows of vias or 'a' is considering the dielectric effect of the material. In this analysis, the via hole value for feeding line and flaring section are constant, also other parameter is not changed except the value of 'a' where the S-parameter and radiation pattern for the varied distance between 2 rows of vias as shown in Figure 3.6 is observed.

3.7 Analysis of flaring angle of SIW sensor

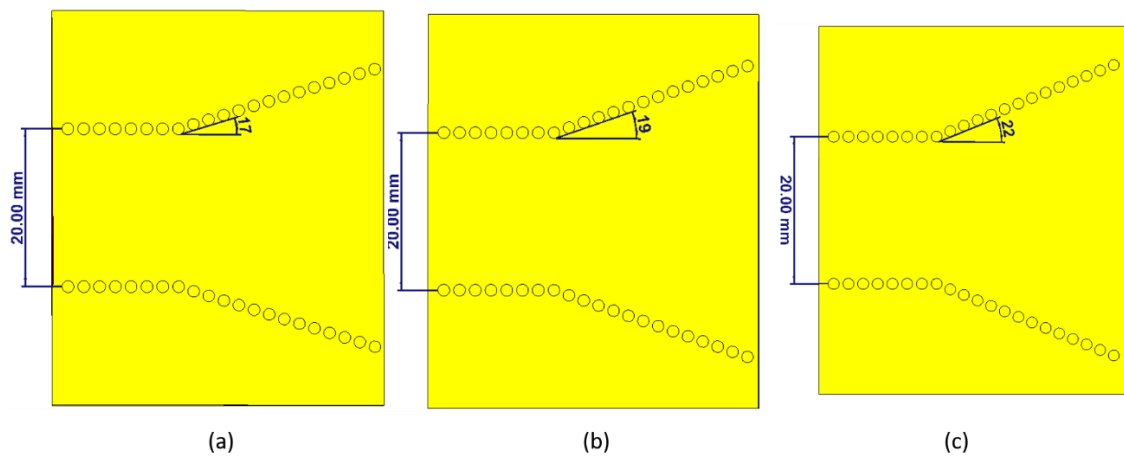


Figure 3.7 Varied value of flaring angle (a) 17° (b) 19° and (c) 22°

In order to improve the performance of SIW sensor, the flaring angle of SIW also analyse by vary the angle from 17°, 19° and 22° as shown in Figure 3.7. The other parameters value are remain constant as mentioned in Table 3.5.

3.8 Analysis of distance between 2 vias (pitch) of SIW sensor

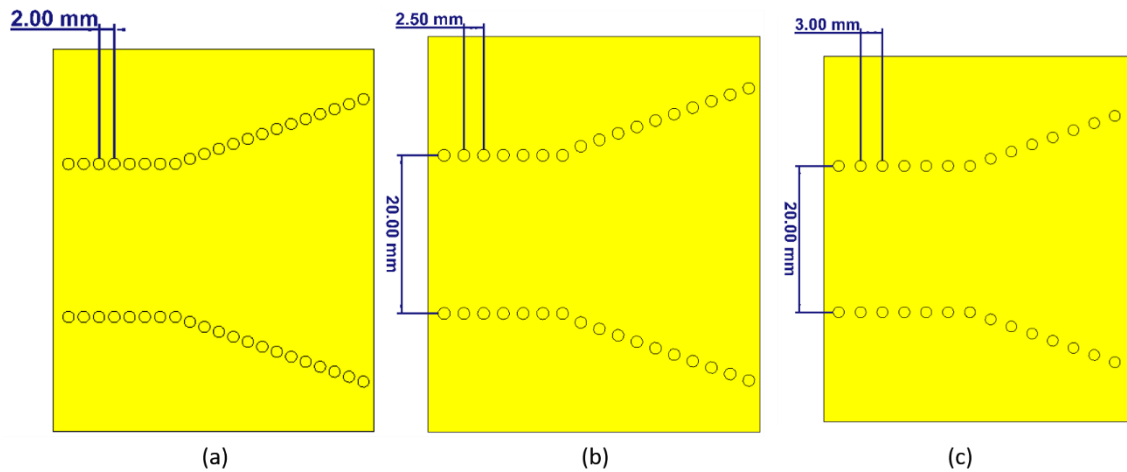


Figure 3.8 Varied value of distance between 2 vias (a) 2mm (b) 2.5mm and (c) 3mm

Another parameter that plays the main role in designing SIW sensor is pitch or distance between 2 vias, where pitch need to be considered in width calculation. There are restriction on determining the pitch value where it should less than diameter of the via hole. In this analysis, the other parameters are remained constant except the length of feeding line and length of flaring section.

Table 3.5 Full dimension of design for 3 analysis above

Parameter	Analysis of 'a'			Analysis of angle			Analysis of pitch		
	1	2	3	1	2	3	1	2	3
Diameter, d (mm)	1.5								
Pitch (Distance between 2 vias), p (mm)	2			2			2	2.5	3
Distance between 2 rows of vias, a (mm)	8	10	20	20			20		
Total height, W (mm)	50								
Length of the feed line, L1 (mm)	14.75			14.75			13.7	15	17.7
Length of the flaring section, L2 (mm)	26.71			26.72	26.71	26.7	24.6	23.3	19.8
Total length, L (mm)	40								
Flaring length (mm)	37.42			35.64	37.42	40.1	37.4	37.4	34.1
Total width (thickness), z s (mm)	1.624								
Aperture angle (°)	19			17	19	22	19		

3.9 Modelling of New SIW Sensor Design

The design in Figure 3.9 is duplicated design from Shibu[30] horn antenna design but with some modification. The configuration with 20mm gap, 20mm loading and no loading are motivated by conventional horn antenna design where the conventional horn antenna design requires transmitter and receiver.

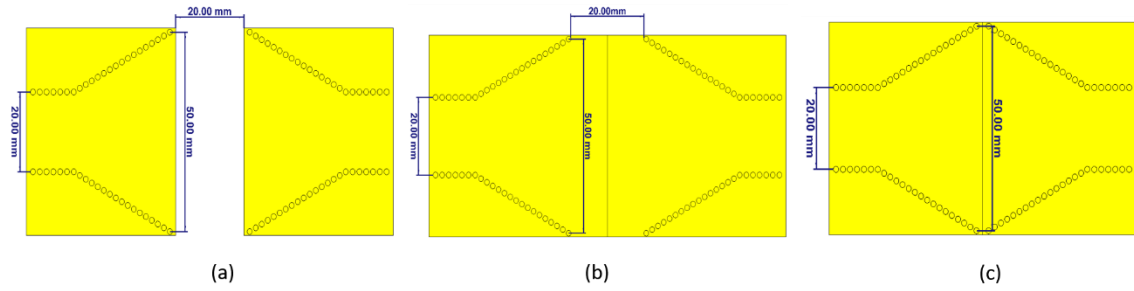


Figure 3.9 Varied configuration of both side horn antenna (a) 20mm gap (b) 20mm loading and (c) no loading

The concept in this thesis is to integrate both transmitter and receiver in the same plate, so idea of the configurations as shown in Figure 3.9 are visualized. The performance result of these 3 configurations is observed and analysed. Table 3.5 stated the full dimension of this configuration.

3.10 Finalize design

The finalize design are motivated by integration of 2 horn antenna SIW sensor with via diameter of 2mm, flaring angle of 17° and distance between 2 rows of vias of 55mm in a single plate which act as transmitter and receiver respectively with a 41.89mm loading to improve the performance. The full dimension of this 3D-Printed SIW sensor using PLA material is as mentioned in Table 3.6.

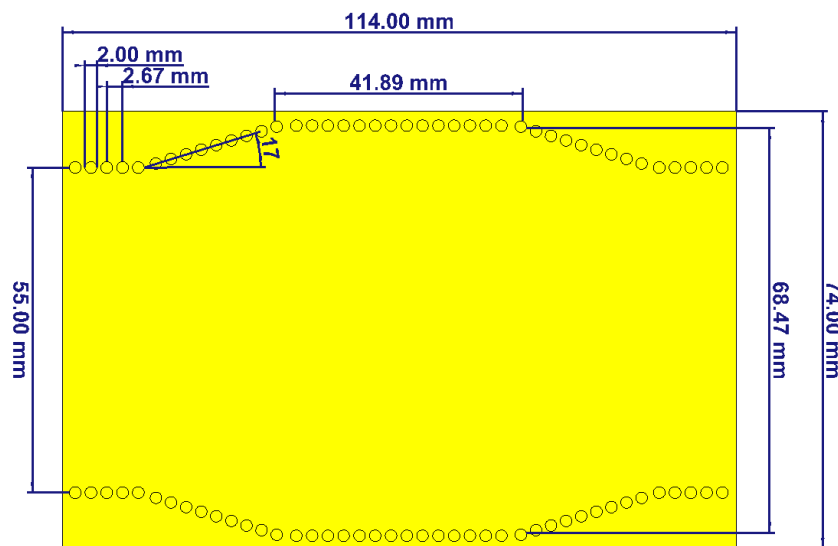


Figure 3.10 Finalize design of SIW sensor

3.11 Chapter Summary

A new design of SIW sensor is developed and modelled in this chapter motivated by Tavin[29] and Shibu [30] design of basic and horn antenna of SIW sensor. Designation process need to considered the new concept proposed and limitation mentioned.

The performance parameter of new develop SIW sensor will be discussed on next chapter.

CHAPTER 4

RESULTS AND DISCUSSIONS

4.1 Introduction

The simulated results for reproduced design and analysis of parameters are presented in this chapter and include the performance parameter such as S-parameter, and radiation pattern in polar.

When the S11 or reflection coefficient is less than -10dB, the design performs well in the S-parameter, indicating that maximum power enters the system and negligible power is reflected before entering the system, whereas S21 should be 0 dB, indicating that no power is reflected from port 2 to port 1. The direction of patterns in radiation patterns is attributed to the waveguide port and attached coaxial probe, which also influences the overall performance.

4.2 Result of Modelling of SIW Sensor

Figure 4.1 shows the simulated S-parameter result for SIW basic structure using CST software. It is measured to have S11 below -10dB between 3.9-10GHz with resonant frequency of 4.1GHz. This result is quite similar to result from Tavin [29] where S11 below -10dB obtained between 4-10GHz with resonant frequency of 4.3GHz and 6.1GHz.

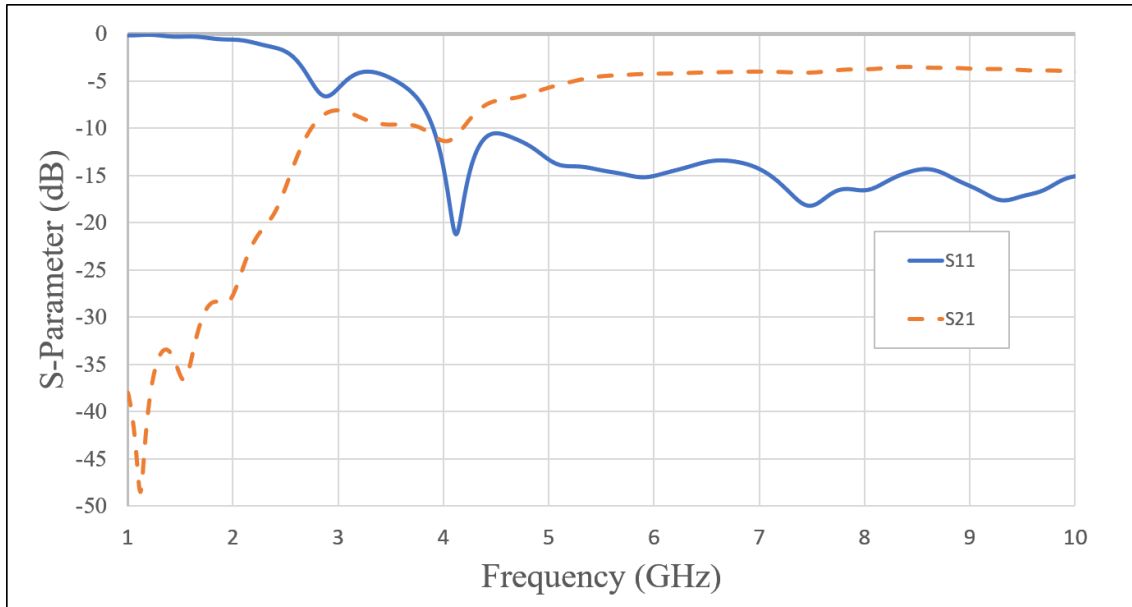


Figure 4.1 Simulated scattering parameter for basic design from [29]

The S-parameter result obtain from Shibu [30] for SIW basic structure is measured to have $S_{11} < -10\text{dB}$ between 6-13GHz with resonant frequency of 6.2GHz, 7GHz, 8.1GHz, 9.3GHz, 10.6GHz and 11.9GHz compared to simulated result obtain as shown in Figure 4.2 is 6-10GHz with resonant frequency of 6.1GHz, 6.9GHz, 7.9GHz and 9GHz.

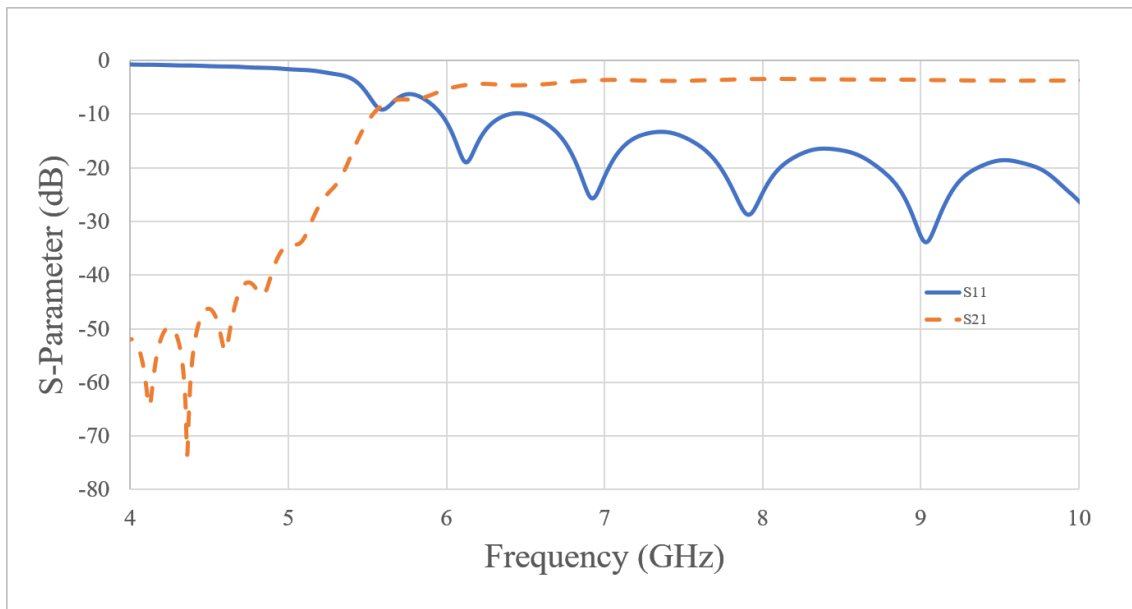


Figure 4.2 Simulated scattering parameter for basic design from Shibu [30]

Figure 4.3 shows the simulated S-parameter result for SIW horn antenna structure in CST software from Tavin [29]. It is measured to have $S_{11} < -10\text{dB}$ between 3.6-3.8GHz with resonant frequency of 3.7GHz while Tavin [29] reported that it is measured to have $S_{11} < -10\text{dB}$ between 3.7-3.9GHz with resonant frequency of 3.8GHz.

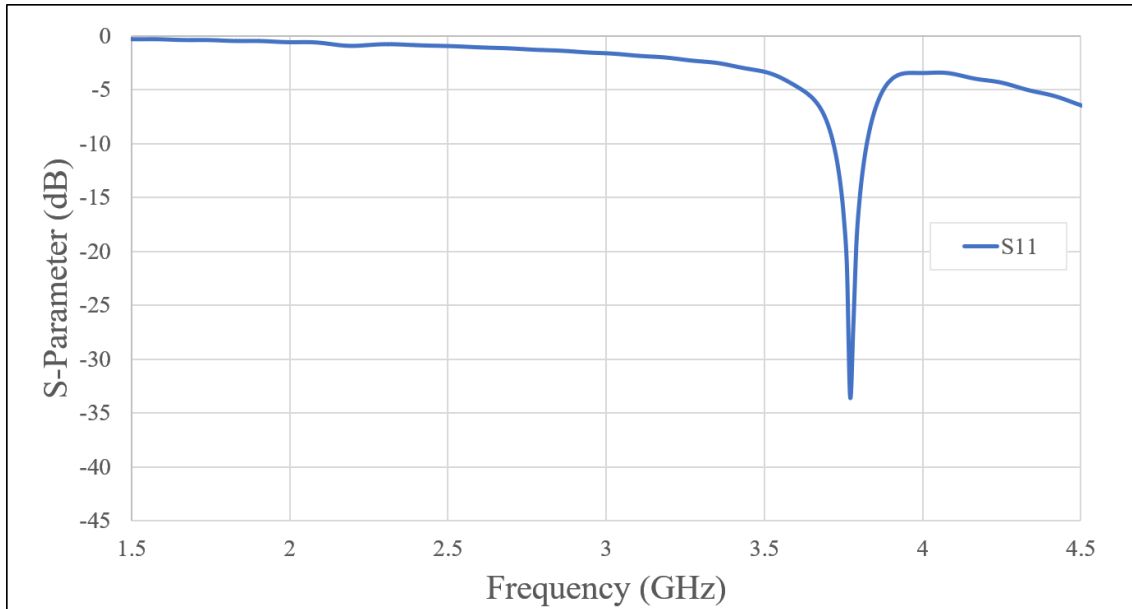


Figure 4.3 Simulated reflection coefficient for horn antenna design from [29] From Tavin [29] research paper, it can be observed that the main beam is directed at an angle of 0° at vertical as shown in Figure 4.4 (a) and is agrees with the simulated result in Figure 4.4 (b).

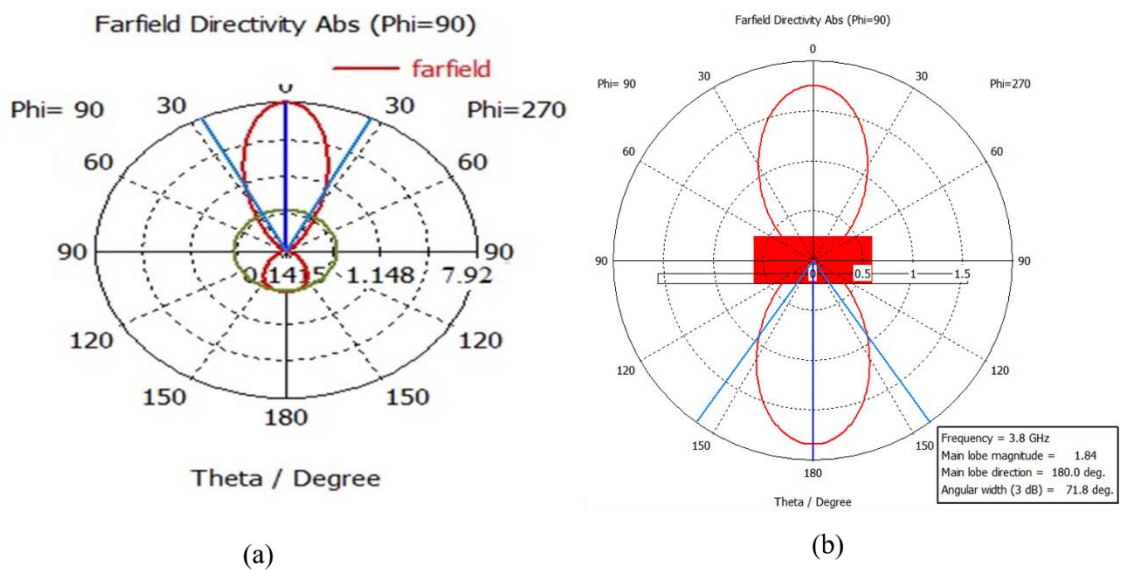


Figure 4.4 Radiation pattern result (a) Tavin [29] (b) simulated

It is measured to have S11 below -10dB in all range of 7-13GHz for the reflection coefficient reported by Shibu [30] and successfully reproduce as shown in Figure 4.5.

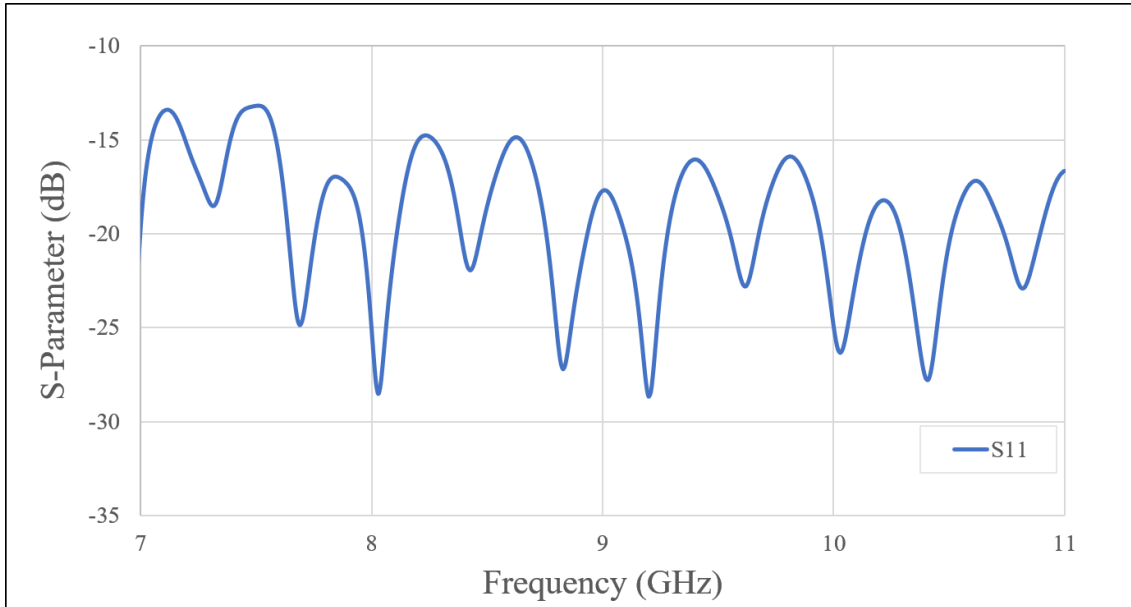


Figure 4.5 Simulated reflection coefficient for horn antenna design from [30]

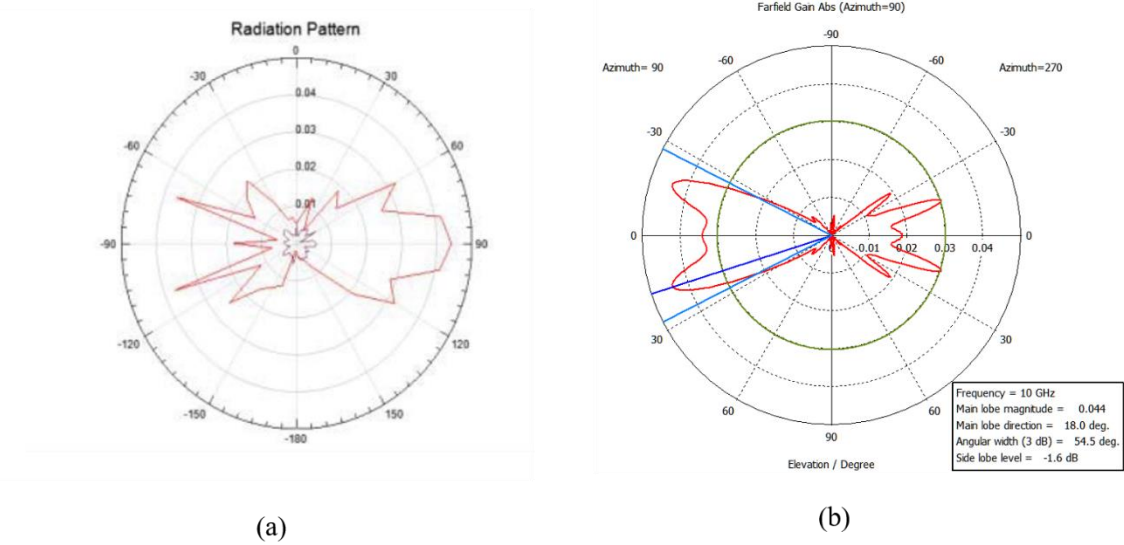


Figure 4.6 Radiation pattern result (a) Shibu [30] (b) simulated

The radiation pattern of horn antenna structure design from Shibu [30] can be observed that the main beam is directed at an angle of 90° to horizontal as shown in Figure 4.6 (a) and at an angle of 0° for simulated result in as shown in Figure 4.6 (b).

After depicting the result from reference papers accurately, thoroughly and precisely following all methodologies used, we want to improve the performance of existing designs by performing a few parameters' analysis.

4.3 Result of Analysis of Distance Between 2 Rows of Vias of SIW Sensor

As stated before, the center-to-center distance between vias in both rows is referred to as 'a.'. From Figure 4.7, the resonant frequency is started at around 4.1GHz at -12.4dB when the value is 20 mm and produce more ripple compared to the value of 10 mm which has maximum magnitude of -20.16dB at 8.85GHz. Meanwhile, the value of 8 mm is not producing any ripple in the range 1-11GHz. From this result, we can conclude that a bigger value of 'a' will lead to the frequency start resonant at a lower frequency.

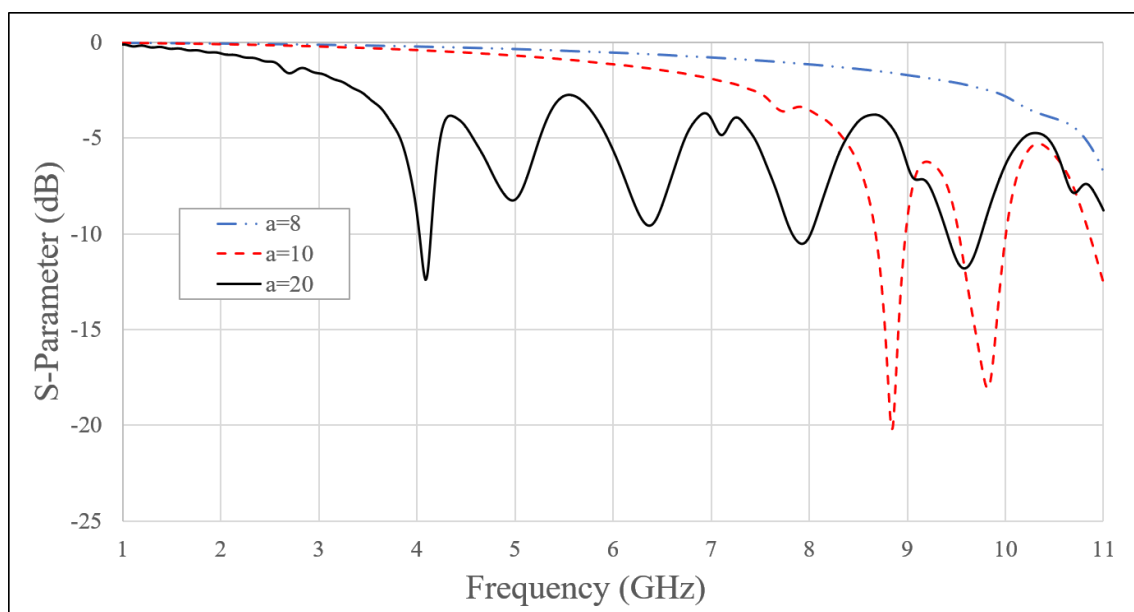


Figure 4.7 Simulated reflection coefficient for varied 'a' value from 8mm, 10mm and 20mm

4.4 Result of Analysis of Flaring Angle of SIW Sensor

The angle in the design is referring to the flaring angle of the horn antenna. As shown in Figure 4.8, the variation value of the angle will affect the ripple. All 3 angles value obtain almost the same magnitude in range of 1-11GHz except for angle of 22° which has additional ripple at 8.73GHz and 10.38GHz with magnitude of -6.3dB and -7.9dB respectively. As the angle increase, the ripples are also increased. But it is not influencing the existing resonant frequency.

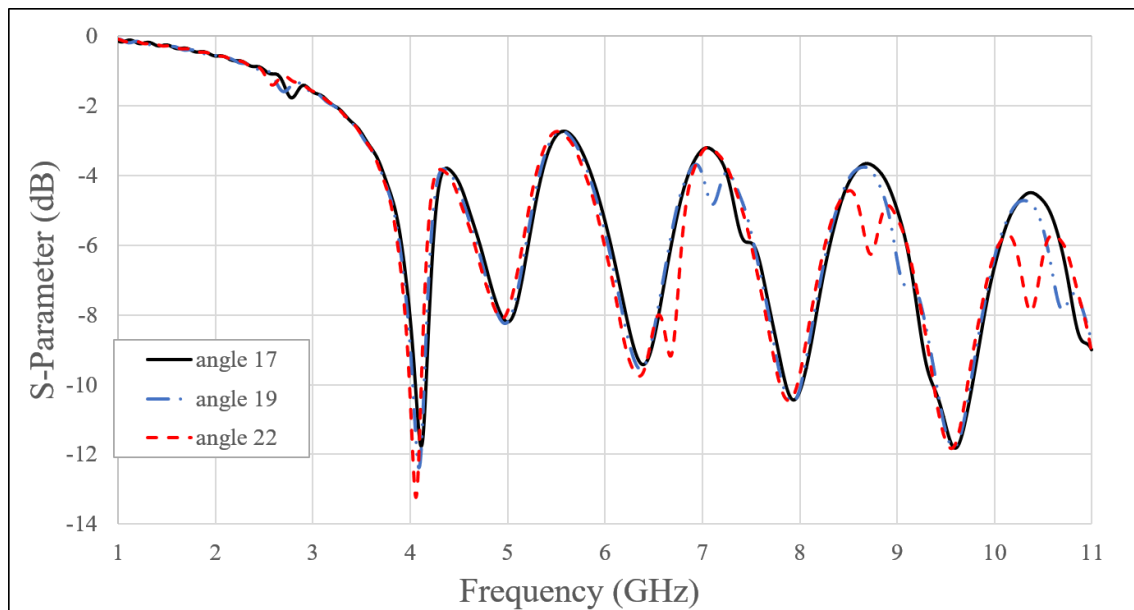


Figure 4.8 Simulated reflection coefficient for varied angle from 17° , 19° and 22° .

4.5 Result of Analysis of Distance Between 2 Via (Pitch) of SIW Sensor

The distance between two metallic vias is called pitch. It can be observed that the pitch values are an important parameter due to the huge changes that happen when the number of pitch is varied. As shown in Figure 4.9, the increment of 1 mm for each change is affecting the whole result. The ripple for pitch value of 1mm initiate at 2.9GHz with magnitude of -4.24dB and achieve highest magnitude of -10.7dB at 9.54GHz compared to pitch value of 3mm with maximum magnitude obtain in this range is -16.4dB at 11GHz. The ripples are increasing, and the magnitude is decreasing when the number of

pitch is increased. While, the ripple is decreasing and the magnitude of the S-parameter is higher when the pitch is small in value.

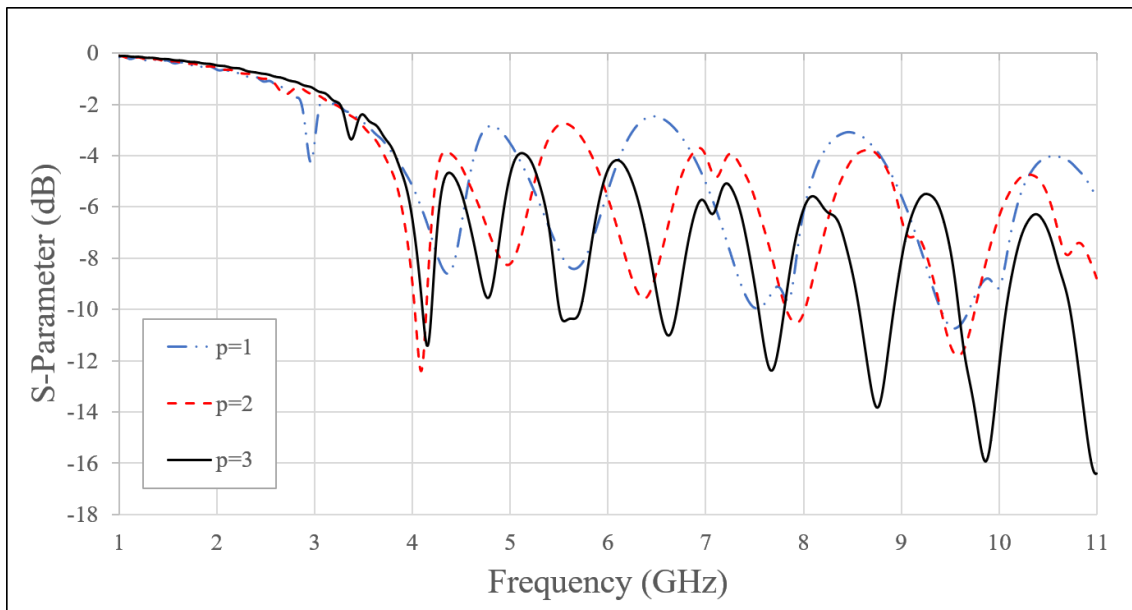


Figure 4.9 Simulated reflection coefficient for varied pitch from 1mm, 2mm and 3mm

4.6 Result of Modelling of New SIW Sensor Design

All 3 configuration can easily differentiate by simulated scattering parameter. As shown in Figure 4.10, Figure 4.11 and Figure 4.12, the configuration with 20mm gap achieve only 2 resonant frequencies at 3.77GHz and 7.42GHz with magnitude of -33.4dB and -40.4dB respectively compared to configuration of 20mm loading which achieve 6 resonant frequencies in range of 4GHz to 8GHz with maximum magnitude of -32.7dB at frequency of 5.67GHz.

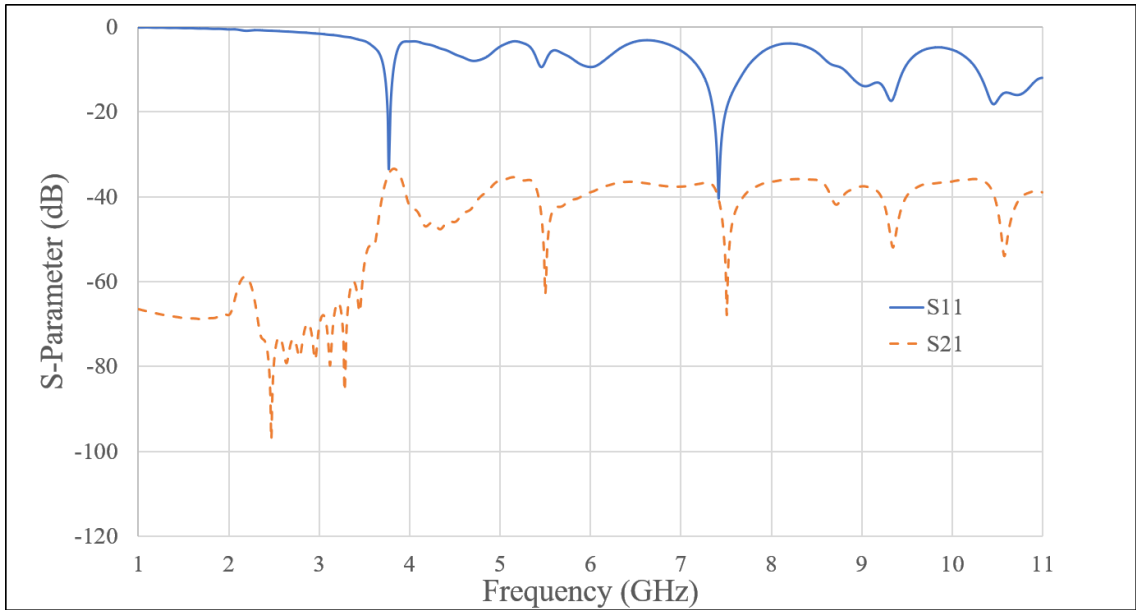


Figure 4.10 Simulated scattering parameter for configuration with 20mm gap

Configuration with no loading simulated scattering parameter as shown in Figure 4.12 also achieve good performance with 2 highest magnitude of -48dB and -41.9dB with frequency of 5.32GHz and 4.45GHz.

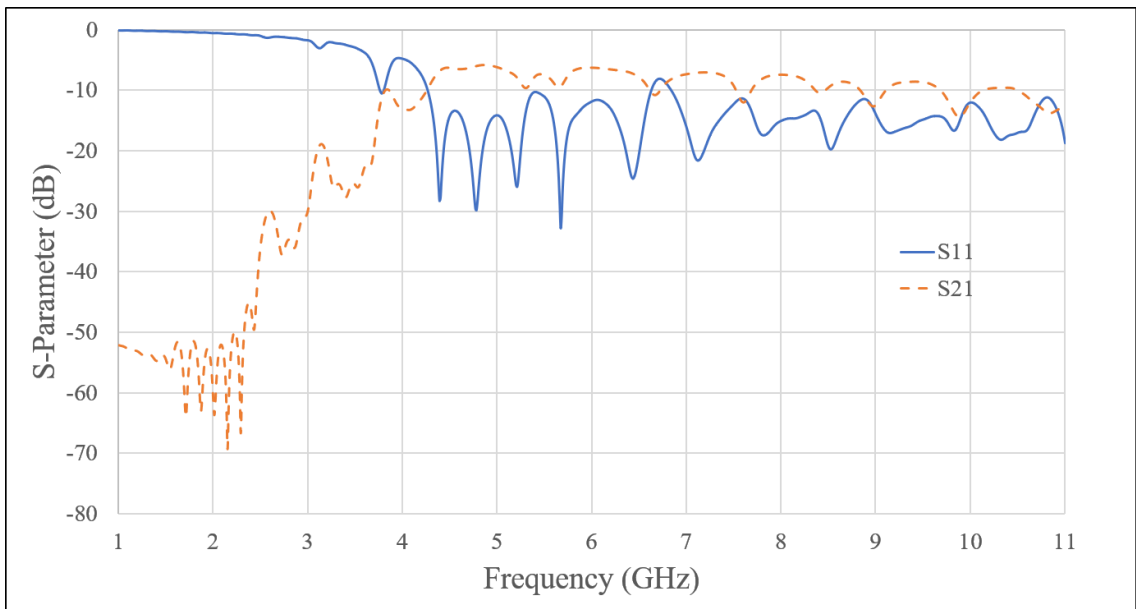


Figure 4.11 Simulated scattering parameter for configuration with 20mm loading

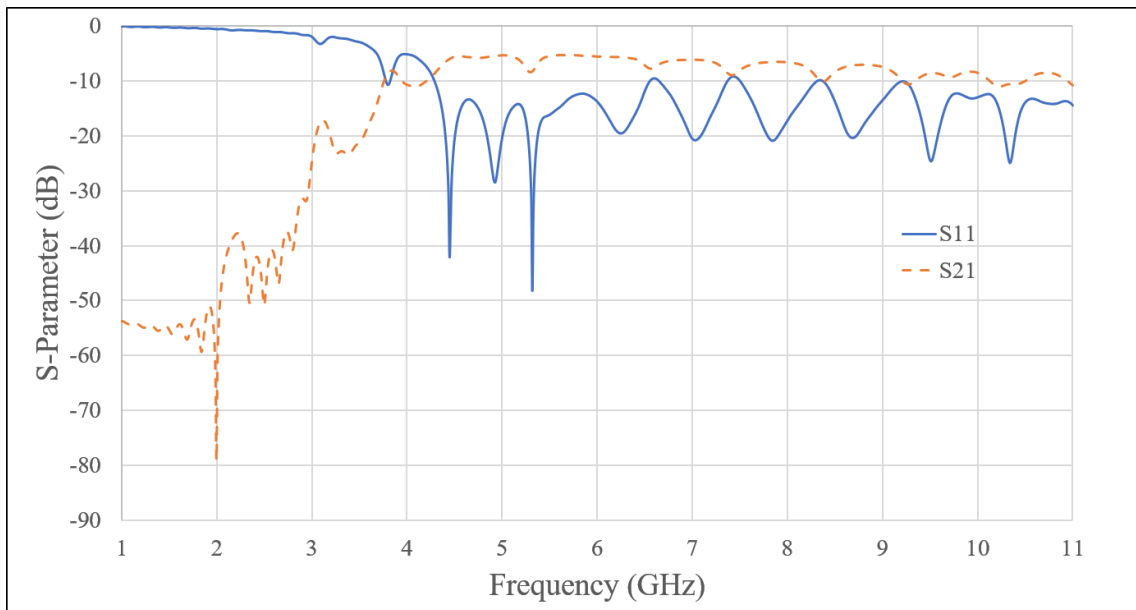


Figure 4.12 Simulated scattering parameter for configuration with no loading
 As the result, from these 3 configurations scattering parameter, the configuration with 20mm loading is better than both with 20mm gap and no loading due to the good ripple in range frequency of 4-6GHz.

4.7 Result of Finalize Design

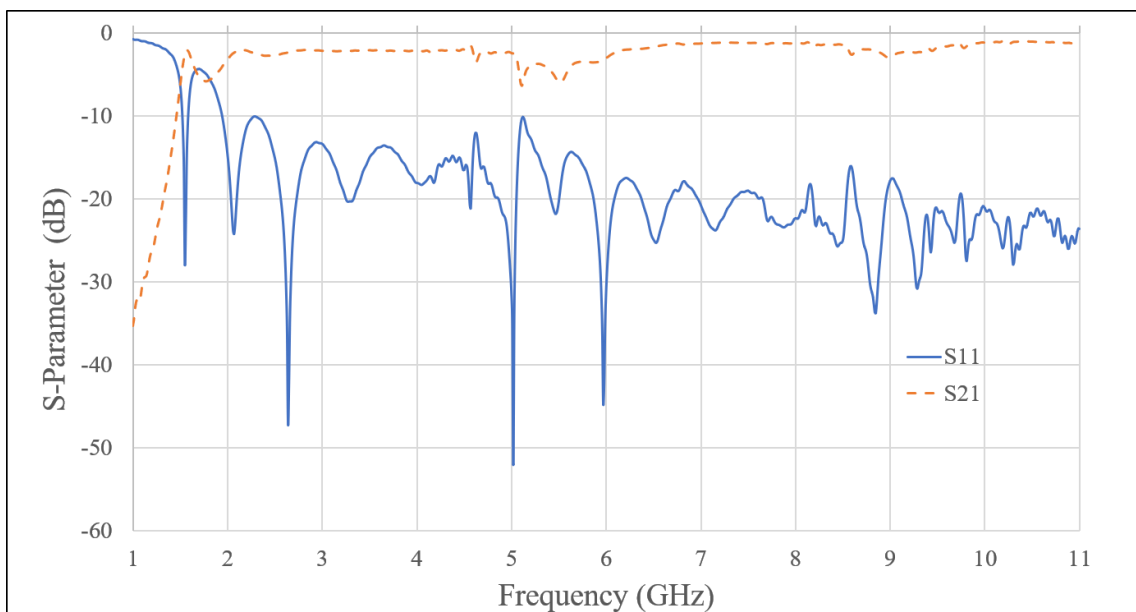


Figure 4.13 Simulated scattering parameter for finalize design

As shown in Figure 4.13, the finalize design using integration of transmitter and receiver in one plate able to achieve good scattering parameter in range of 4-6GHz where the resonant frequency is 5GHz and 6GHz with magnitude of -52dB and -44.3dB respectively.

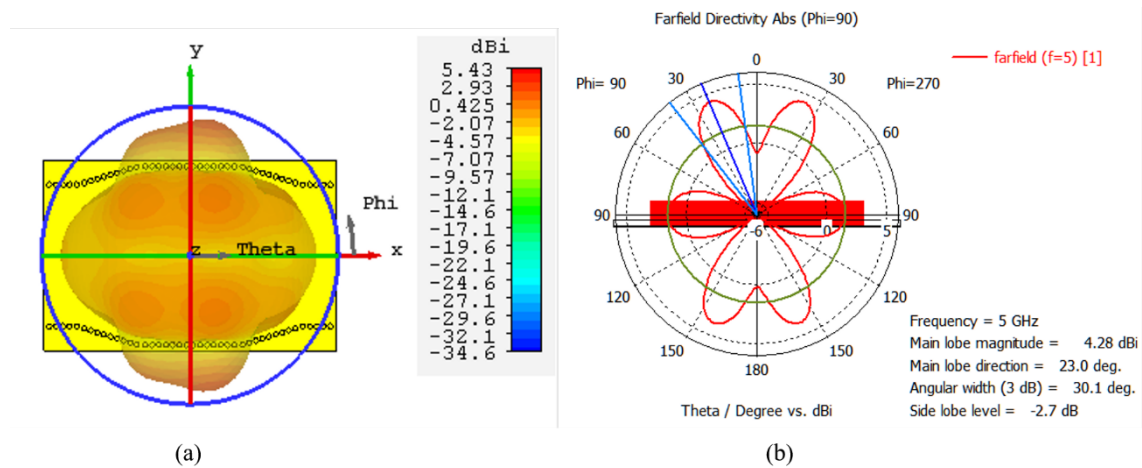


Figure 4.14 Radiation pattern in (a) 3D and (b) polar for finalize design at 5GHz. The radiation pattern achieve also shows the good performance as the main lobe magnitude is in positive range, 4.28dBi with low side love level, -2.7dB.

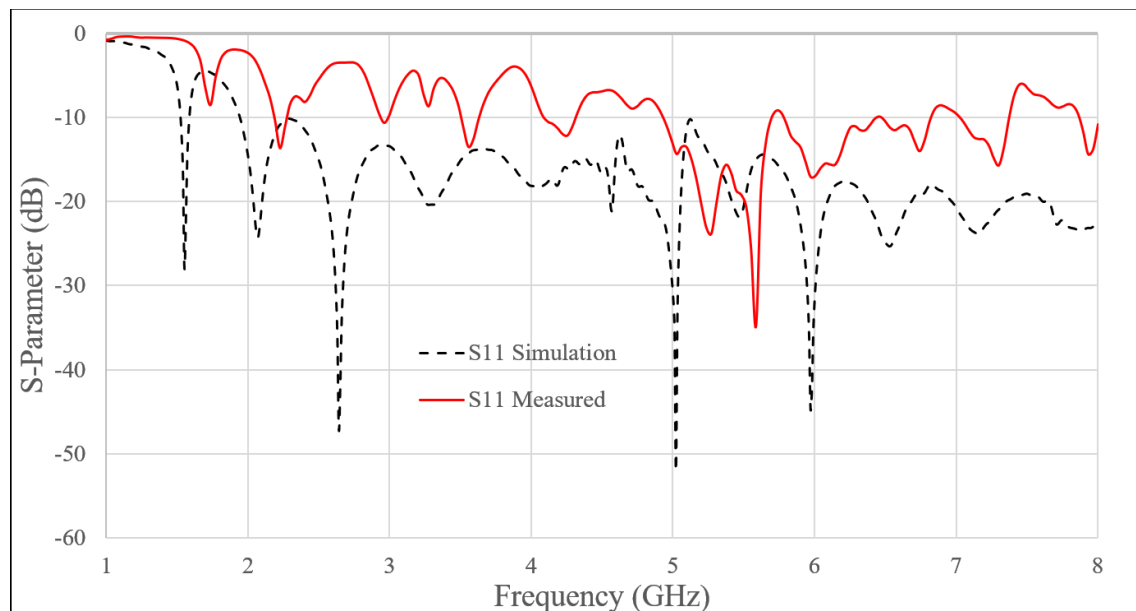


Figure 4.15 Simulated (dashed line) and measured (solid line) reflection coefficient for finalize design

Fabrication process is done using PLA material using 3D printer which may causes the slightly difference between simulated and measured scattering parameter result. As presented in Figure 4.15, the measured scattering parameter able to achieve one resonant frequency at 5.6GHz with magnitude of -35dB.

4.8 Chapter summary

At the end of this chapter, a new develop SIW sensor is successfully fabricated and measured. The scattering result is good and all objectives achieved. The process of reproduced design, the result from simulated result represented and is agreed when compared to the original SIW basic and horn antenna structures. Next, the analysis for three parameters was observed, which is the 'a', angle and pitch. The analysis results are also discussed in this chapter.

CHAPTER 5

CONCLUSION

5.1 Conclusion

For conclusion, all objectives are achieved successfully. The modelling of SIW sensor using CST software by validating technique from previous research paper showing the positive result as the simulated result are same as in the research paper. Next, analysing of parameter performance are done to achieve appropriate and suitable parameter in geometrical term before the development of new design.

The final design incorporates a concept that allows the transmitter and receiver to be integrated onto one plate are successfully achieve which allowing for good scattering parameters in the 4-6GHz band, with resonance frequencies of 5GHz and 6GHz having magnitudes of -52dB and -44.3dB, respectively.

REFERENCES

1. T. Djerafi, A. Doghri, and K. Wu, "Substrate Integrated Waveguide Antennas." Handbook of Antenna Technologies, pp. 1-60, 2015, doi: 10.1007/978-981-4560-75-7_57-1.
 2. T. Djerafi, A. Doghri, and K. Wu, "Substrate Integrated Waveguide Antennas." Handbook of Antenna Technologies, pp. 1-60, 2015, doi: 10.1007/978-981-4560-75-7_57-1.
 3. Jilani, Muhammad Taha. (2012). A Brief Review of Measuring Techniques for Characterization of Dielectric Materials. International Journal of Information Technology and Electrical Engineering.
 4. Z. Chen and H. Meng, "A Novel Dielectric Constant Measurement Method Based on SIW Slot Array Antenna," 2020 International Conference on Microwave and Millimeter Wave Technology (ICMMT), 2020, pp. 1-3, doi: 10.1109/ICMMT49418.2020.9386779.
 5. S. L. S. Severo, Álvaro A. A. de Salles, B. Nervis, and B. K. Zanini, "Non-resonant Permittivity Measurement Methods." Journal of Microwaves, Optoelectronics and Electromagnetic Applications, vol. 16, no. 1, pp. 297-311, 2017, doi: 10.1590/2179-10742017v16i1890.
- M. Sharma and H. Singh, "SIW based Leaky wave antenna with Semi C-shaped slots and its Modeling, Design and parametric considerations for different materials of Dielectric," 2018 Fifth International Conference on Parallel, Distributed and Grid Computing (PDGC), 2018, pp. 252-258, doi: 10.1109/PDGC.2018.8745966.
6. Xuan Hui Wu; Ahmed Kishk, Analysis and Design of Substrate Integrated Waveguide Using Efficient 2D Hybrid Method, Morgan & Claypool, 20
- Erwanto, Y., Rohman, A., Arsyanti, L., & Pranoto, Y. (2018). Identification of pig DNA in food products using polymerase chain reaction (PCR) for halal authentication-a review. International Food Research Journal, 25(4), 1322–1331.
7. K. Fenske and D. Misra, "Dielectric Materials at Microwave Frequencies," Appl. Microw. Wirel., no. 2, 2000.
 8. R. Jamal, T. Olivier, D. Nicolas, and V. Serge, "Non-destructive microwave characterization and imaging of dielectric materials using a near field technique," Mediterr. Microw. Symp., pp. 0–3, 2013, doi: 10.1109/MMS.2013.6663074.
- A. A. Mohd Azoddein, R. B. Mohd Yunus, N. M. Nik Sulaiman, and A. B. Bustary, "Effect of Mercury concentration on *P. putida* growth in Mercury removal." Journal of Applied and Physical Sciences, vol. 3, no. 3, pp. 107-116, 2017, doi: 10.20474/japs-3.3.4.
9. A. Verma and D. C. Dube, "Measurement of dielectric parameters of small samples at X-band frequencies by cavity perturbation technique," IEEE Trans. Instrum. Meas., vol. 54, no. 5, pp. 2120–2123, 2005, doi: 10.1109/TIM.2005.854249.

10. C. Balanis. (2005) *Antenna theory*. New York: Wiley-Interscience.
- Erwanto, Y., Rohman, A., Arsyanti, L., & Pranoto, Y. (2018). Identification of pig DNA in food products using polymerase chain reaction (PCR) for halal authentication-a review. *International Food Research Journal*, 25(4), 1322–1331.
11. T. Djerafi, A. Doghri, and K. Wu, “Substrate Integrated Waveguide Antennas.” *Handbook of Antenna Technologies*, pp. 1-60, 2015, doi: 10.1007/978-981-4560-757_57-1.
12. Z. L. Li and K. Wu, “A new approach to integrated horn antenna,” in *Proc. Int. Symp. Antenna Technol. Appl. Electromagn.*, pp. 535–538, Jul. 2004
13. Nayak, A. K., & Patnaik, A. (2018). Design of an SIW corrugated H-plane horn antenna with improved performance. *Applied Electromagnetics Conference, AEMC 2017, 2018-January*, 1–2. <https://doi.org/10.1109/AEMC.2017.8325734>
- W. Q. Che, B. Fu, P. Yao, Y. L. Chow, and E. K. N. Yung, “A compact substrate integrated waveguide H-plane horn antenna with dielectric arc lens: Research articles,” *Int. J. RF Microw. Comput.-Aided Eng.*, vol. 17, Sep. 2007, pp. 473–479
14. Wong M, Sebak AR, Denidni TA (2008) A broadside substrate integrated horn antenna. In: *IEEE AP-S international symposium 2008, Atlanta*, pp 1–4
15. Geyi, W. (2010). *Antenna Theory*. In *Foundations of Applied Electrodynamics*. <https://doi.org/10.1002/9780470661369.ch4>
16. Morote, M. E. (2014). *Horn Antennas and Dual-Polarized Circuits in Substrate Integrated Waveguide (SIW) Technology*. 6421, 1–177.
- Wang H, Fang D-G, Zhang B, Che W-Q (2010) Dielectric loaded substrate integrated waveguide (SIW) H-plane horn antennas. *IEEE Trans Antennas Propag* 58(3):640–647
17. N. K. Tiwari and M. J. Akhtar, “Partially Filled Substrate Integrated Waveguide-Based Microwave Technique for Broadband Dielectric Characterization,” *IEEE Trans. Instrum. Meas.*, vol. 68, no. 8, pp. 2907–2915, 2019, doi: 10.1109/TIM.2018.2871807.
18. P. K. Varshney and M. J. Akhtar, “Permittivity estimation of dielectric substrate materials via enhanced siw sensor,” *IEEE Sens. J.*, vol. 21, no. 10, pp. 12104–12112, 2021, doi: 10.1109/JSEN.2021.3064923.
19. Y. Xiang, J. Huang, L. Fu, Y. Chen, W. Gu, and Y. Wu, “A Folded Substrate Integrated Waveguide Re-Entrant Cavity for Full Characterization of Magneto-Dielectric Powder Materials,” *IEEE Sens. J.*, vol. 21, no. 9, pp. 10657–10666, 2021, doi: 10.1109/JSEN.2021.3063518.
- D. Q. Sun, J. P. Xu, and S. Jiang, “SIW horn antenna built on thin substrate with improved impedance matching,” *Electron. Lett.*, vol. 51, no. 16, pp. 1233–1234, Aug. 2015.
20. A. K. Jha and M. J. Akhtar, “SIW cavity based RF sensor for dielectric characterization of liquids,” *2014 IEEE Conf. Antenna Meas. Appl. CAMA 2014*, 2014, doi: 10.1109/CAMA.2014.7003427.

21. M. F. Cordoba-Eraza and T. M. Weller, "Liquids characterization using a dielectric resonator-based microwave probe," *Eur. Microw. Week 2012 "sp. Microwaves", EuMW 2012, Conf. Proc. - 42nd Eur. Microw. Conf. EuMC 2012*, pp. 655–658, 2012, doi: 10.23919/eumc.2012.6459087.
22. A. Savić, N. Meyne, and A. F. Jacob, "Microwave impedance sensors for the dielectric characterization of liquids," *GeMiC 2018 - 2018 Ger. Microw. Conf.*, vol. 2018-January, pp. 219–222, 2018, doi: 10.23919/GEMIC.2018.8335069.
23. A. K. Jha and M. J. Akhtar, *Design of microwave ENZ sensor for contamination detection in liquids using SIW technology*. 2014.
24. M. E. Morote, B. Fuchs, J. F. Zurcher, and J. R. Mosig, "A printed transition for matching improvement of SIW horn antennas," *IEEE Trans. Antennas Propag.*, vol. 61, no. 4, pp. 1923–1930, Apr. 2013.
25. S. W. Yik, "Design of integrated rectangular SIW filter microstrip patch antenna for wireless communications," 2014, [Online]. Available: <http://eprints.utm.edu.my/15006/>.
26. Cai, Y., Yingsong, Z., Yang, L., Jing, N., & Qian, Z. (2016). Improvement of SIW horn antenna with metallic via drilled transition. 2016 IEEE MTT-S International Microwave Workshop Series on Advanced Materials and Processes for RF and THz Applications, IMWS-AMP 2016 - Proceeding, 15–17. <https://doi.org/10.1109/IMWS-AMP.2016.7588386>
27. B. J. Creech, "S-Parameters Allow High-Frequency Verification of RF Switch Models," pp. 10–13, 2011.
28. Xuan Hui Wu; Ahmed Kishk, *Analysis and Design of Substrate Integrated Waveguide Using Efficient 2D Hybrid Method*, Morgan & Claypool, 2010.
29. T. Agrawal, "Two Element MIMO Antenna using Substrate Integrated Waveguide (SIW) Horn," vol. 1, pp. 508–511, 2016.
30. H. X. H. Antenna, "Horn Antenna using Substrate Integrated Waveguide," pp. 661–664, 2016.